

Review

# Physicochemical Parameters and Geochemical Features of Ore-Forming Fluids for Orogenic Gold Deposits Throughout Geological Time

Vsevolod Yu. Prokofiev <sup>1,\*</sup>  and Vladimir B. Naumov <sup>2</sup><sup>1</sup> Institute of Geology of Ore Deposits, Petrography, Mineralogy, and Geochemistry, Russian Academy of Sciences, Moscow 119017, Russia<sup>2</sup> Vernadsky Institute of Geochemistry and Analytical Chemistry, Russian Academy of Sciences, Moscow 119991, Russia; naumov@geokhi.ru

\* Correspondence: vpr@igem.ru

Received: 2 December 2019; Accepted: 2 January 2020; Published: 5 January 2020



**Abstract:** This paper reviews data from numerous publications focused on the physicochemical parameters and chemical composition of ore-forming fluids from orogenic gold deposits formed during various geological epochs. The paper presents analysis of the distribution of the principal parameters of mineralizing fluids depending on the age of the mineralization. Some parameters of the fluids (their salinity and pressure) at orogenic gold deposits are demonstrated to systematically vary from older (median salinity 6.1 wt.%, median pressure 1680 bar) to younger (median salinity 3.6 wt.%, median pressure 1305 bar) deposits. The detected statistically significant differences between some parameters of mineralizing fluids at orogenic gold deposits are principally new information. The parameters at which mineralization of various age was formed are demonstrated to pertain to different depth levels of similar mineralization-forming systems. The fluid parameters of the most ancient deposits (which are mostly deeply eroded) correspond to the deepest levels of orogenic fluid systems. Hence, the detected differences in the salinity and pressure of the mineralizing fluids at orogenic deposits of different age reflect the vertical zoning of the mineralizing fluid systems.

**Keywords:** orogenic gold deposit; mineralizing fluid; fluid inclusions; temperature; salinity; pressure; age; zonation

## 1. Introduction

Orogenic gold deposits are one of the world's main groups of gold deposits that provide a source of gold ([1], etc.). Deposits of this class are formed in deformed and metamorphosed crustal blocks and terranes, typically in greenschist facies rocks adjacent to major crustal fault zones. Orogenic gold deposits were generated during a time span of more than 3 byr, from the Precambrian throughout the whole Phanerozoic [2]. It is thus interesting to understand how, and how much, the fluid regime (i.e., the physicochemical parameters and chemical composition of mineral-forming fluids) evolved over the Earth's history when these deposits were formed.

To do this, we examined a database [3] that currently contains data compiled from a large quantity of publications on mineral-hosted fluid inclusions. Before these data were entered into the database, we tested them for suitability and reliability. Data on mineral-hosted fluid inclusions from gold deposits have been reported extensively in the economic geology literature during the past four to five decades. This information includes estimates of the composition and P–T parameters of the mineral-forming fluids, but also the age of the ore-forming processes. We analyzed these parameters in the database, as well as associated information on the volatile composition of orogenic gold-forming fluids for which

reliable isotopic or geological age data were available. We have gathered information on more than 300 orogenic gold deposits of different age from 186 publications (Table 1), which illustrates how informative are our data on the physicochemical parameters of fluids for the whole class of orogenic gold deposits. More than 3500 conjugated estimations of homogenization temperatures and fluid salinities and more than 1100 conjugated estimations of temperatures and pressures are collected. Tables 2–7 provides information on the range of variations in fluid temperatures, salinity and pressures, the number of inclusions studied, and the chemical composition of the fluid. The deposits discussed herein (Table 1) were subdivided into the following five age groups: Meso-Neoarchean (3200–2500 Ma), Paleoproterozoic (2500–1600 Ma), Meso- and Neoproterozoic (1600–540 Ma), Paleozoic (540–250 Ma), Mesozoic (250–65 Ma), and Cenozoic (65–0 Ma). It is necessary to mention that data on Neo- and Mesoproterozoic gold deposits are relatively scarce; hence, we were not able to analyze this time span in more detail.

The parameters for the PTX of the fluids in the comprehensive database are for individual samples, if this information is available from the respective papers. In cases where many values for inclusion homogenization temperatures were reported for a given sample, the database presents an average value for the sample if the difference between the maximum and minimum temperature values is less than 50 °C. If this difference is equal to or greater than 50 °C, then both the maximum and the minimum temperature values are reported. Analogously, for the salinity measurements, we assume average values if the difference is less than 5 wt.% and use the maximum and minimum values if the difference is greater. For fluid pressure, average values are used if the difference is smaller than 10%, and, otherwise, the maximum and minimum values are reported.

Some publications on multiphase fluid inclusions containing saturated chloride brines quote homogenization temperatures as those when the gas bubble dissolved in the inclusion, despite the halite phase dissolving at a higher temperature. Because salinities in these inclusions were calculated from the NaCl solubility relationships, in the publications lacking reported halite dissolution temperatures, these data fall behind the saturation curve of aqueous solution with sodium chloride. To transform information on such inclusions into a reasonably accurate form, we quote their homogenization temperatures as the calculated homogenization temperatures of a saturated NaCl solution whose concentration is as specified in the paper.

## 2. Brief Description of the Deposits

For our analysis, we have selected deposits at which the arrangement of mineralized veins is controlled by tectonics. These are mostly deposits hosted in sedimentary or metamorphic rocks. The deposit was included in the sample if its geological characteristics did not contradict to the attributes of orogenic gold deposits formulated in the classical work [4]. In controversial cases, we included a deposit in the number of orogenic ones if it was considered orogenic in the review works of authoritative scientists, for example [5]. The resources and reserves of these deposits broadly vary from small (<10 tonnes) to superlarge (>1000 tonnes). In Table 1, deposits printed in bold face have gold reserves of 100 tonnes or more, and data for these were analyzed separately to determine what fluid parameters, if any, led to formation of such large deposits. Deposits data on which are absent from Table 1 are small- and medium-sized ones.

The evaluated gold deposits are listed in Table 1 in ascending order of their age (e.g., from younger to older) and, within a given epoch, in the chronological order of the publications, with data on the parameters and composition of the fluids.

Among the **Cenozoic** deposits, we discuss those in the United States, Canada, Italy, Austria, New Zealand, China, Iran, Georgia Republic, and Mexico. The data were compiled from nineteen publications and pertain to 26 gold deposits. Some of these deposits are large: Alaska-Juneau (USA), Bralorne-Pioneer (Canada), La Herradura (Mexico), and Daping (China).

The **Mesozoic** deposits are located in the United States, China, Korea, New Zealand, Russia, Mongolia, and Honduras. The data were borrowed from 70 publications and characterize

155 gold deposits. Among these, the following deposits are large: Samdong and Gubong (Korea), Dongping, Linglong, Wenyu, Sanshandao, Dongfeng, Taishang, Luoshan, and Jinshan (China), Kyuchus, Mayskoye, Nezhdaninskoye, Arkachan, Natalkinskoye (Russia), and Donlin Creek (USA).

The **Paleozoic** deposits occur in Australia, Kazakhstan, Peru, Russia, Uzbekistan, France, and Portugal. The data are from 33 publications and characterize 53 gold deposits. The large deposits are Zholymbet, Bestobe, S. Aksu, and Vasilkovskoye, (Kazakhstan), Zarmitan (Uzbekistan), Sukhoi Log, Verninskoye and Berezovskoye (Russia), and Bendigo, Charters Towers, and Telfer (Australia).

The **Meso- and Neoproterozoic** deposits are known in Russia, Brazil, Sweden, Australia. The data were extracted from seven publications and characterize twelve gold deposits. The large deposits among these are Olimpiadinskoye and Veduga (Russia), and Telfer (Australia).

The **Paleoproterozoic** deposits are known in Canada, Finland, Brazil, Australia, Sweden, West Africa, Mali, and Ghana. The data were collected from 22 publications and characterize 29 gold deposits. The large deposits among these are Callie (Australia), Morila and Yalea (Mali), and Piaba (Brazil).

**Meso-Neoarchean** deposits of this type are known in Canada, India, South Africa, Australia, Finland, and Zimbabwe. The data were taken from 33 publications and pertain to 35 gold deposits. The large deposits include McIntyre-Hollinger, Sigma, Pamour, Surluga, and Giant (Canada), Kolar, Hutt, Uti, and Hira-Buddini (India), and Wiluna, Junction, Golden Mile/Mount Charlotte, and Tarmoola (Australia).

Note that many of these deposits are world-class gold deposits with >100 tonnes Au. These giants include the ore fields of Kolar, India; Telfer, Bendigo, and Kalgoorlie, Australia; McIntyre-Hollinger, Canada; Vasilkovskoye, Zarmitan, Muruntau, and Kumtor, Central, Asia; Sanshandao and Linglong, China; and Natalkinskoye, Olimpiadinskoye, and Sukhoi Log, Russia.

**Table 1.** Orogenic gold deposit.

Deposition *, Country	Province	Gold Content, Moz (Million Ounces)	Gold Content, Metric Tons	Age, Ma	Reference
<b>Cenozoic</b>					
Valdez Group, USA	South-central Alaska	0.26	8	50–55	[6]
Venus, Canada	Yukon Territory	<0.16	<5	70	[7]
Monte Rosa gold district, Italy	Northwestern Alps	0.5	15	20	[8]
Fairview, Oro Fino, Canada	Okanagan Valley, British Columbia	2.2	68	Tertiary	[9]
Twin Lakes, Canada	Okanagan Valley, British Columbia	0.01	0.27	Tertiary	[9]
Alaska-Juneau, USA	Juneau Gold Belt, Alaska	3.4	106	55	[10]
Ibex, USA	Juneau Gold Belt, Alaska	<0.3	<10	55	[10]
Reagan, USA	Juneau Gold Belt, Alaska	<0.3	<10	55	[10]
Treadwell, USA	Juneau Gold Belt, Alaska	3.1	96	55	[10]
Bralorne-Pioneer, Canada	British Columbia	4.1	129	65	[11]
Monte Rosa gold district, Italy	Northwestern Alps	0.5	15	24–32	[12]
Bralorne-Pioneer, Canada	British Columbia	4.1	129	65	[13]
Callery, New Zealand	BDT	<0.16	<5	Quaternary	[14]
Shotover, New Zealand		<0.16	<5	Miocene	[14]
Mt. Alta, New Zealand		<0.16	<5	Miocene	[14]
Nenthorn, New Zealand		<0.16	<5	Paleocene–Eocene	[14]
Böckstein, Austria	Northwestern Alps	<0.16	<5	Tertiary	[15]
Monte Rosa gold district, Italy	Northwestern Alps	0.5	15	24–32	[15]
Kensington, USA	Berners Bay District, Southeast Alaska	1.9	60	55	[16]
Jualin, USA	Berners Bay District, Southeast Alaska	0.3	9	55	[16]
Shannan area China	S. Tibet	0.96	30	Eocene	[17]
Muteh, Iran	Zagros	0.45	14	38.5–55.7	[18]
Zopkhito, Georgia Republic	Greater Caucasus	1.8	55	4–5	[19]
La Herradura, Mexico	Northwestern Mexico	5.4	168	61.0 ± 2.1	[20]
Daping, China	Yunnan Province	>4.8	>150	Cenozoic	[21]
Mayum, China	Tibet	>2.6	>80	59	[22]
Zhemulang, China	Lang County, Tibet	<0.16	<5	12–35	[23]
Mazhalia, China	Cuomei County, Tibet	<0.16	<5	12–35	[23]
Qolqoleh, Iran	Sanandaj-Sirjan Zone, Kurdistan Province	<0.3	<10	Early Tertiary	[24]
Bangbu, China	Southern Tibet	1.3	40	Cenozoic	[25]
<b>Mezocoic</b>					
Oriental mine, USA	California	0.15	4.7	120	[26]
Big Hurrah, USA	Alaska	<0.3	<1	110	[27]
Mouther Lode, USA	California	1.7	53	125	[28]
Yata, China	Guizhou, Youjiang basin, S. China	0.32	10	182–206	[29]
Daeil, Korea	Youngdong dist.	-	-	145	[30]
Macraes, New Zealand		-	-	Cretaceous	[14]

Table 1. Cont.

Deposition *, Country	Province	Gold Content, Moz (Million Ounces)	Gold Content, Metric Tons	Age, Ma	Reference
<b>Mezocoic</b>					
Glenorchy, New Zealand		-	-	Cretaceous	[14]
Barewood, New Zealand		-	-	Cretaceous	[14]
Bendigo, New Zealand		-	-	Cretaceous	[14]
Bonanza, New Zealand		-	-	Cretaceous	[14]
Quartz Hill, USA	California	0.1	3.7	150	[31]
Lover Dominion, Canada	Klondike, Yukon Territory	-	-	160	[32]
Aime, Canada	Klondike, Yukon Territory	-	-	160	[32]
Gold Run, Canada	Klondike, Yukon Territory	-	-	160	[32]
Portland Creek, Canada	Klondike, Yukon Territory	-	-	160	[32]
Lloid, Canada	Klondike, Yukon Territory	-	-	160	[32]
Hunker Dome, Canada	Klondike, Yukon Territory	-	-	160	[32]
Mitchell, Canada	Klondike, Yukon Territory	-	-	160	[32]
Sheba, Canada	Klondike, Yukon Territory	2.2	69	160	[32]
Lone Star, Canada	Klondike, Yukon Territory	-	-	160	[32]
Hilchey, Canada	Klondike, Yukon Territory	-	-	160	[32]
27 Pup, Canada	Klondike, Yukon Territory	-	-	160	[32]
Violet, Canada	Klondike, Yukon Territory	-	-	160	[32]
Virgin, Canada	Klondike, Yukon Territory	-	-	160	[32]
Amethyst, Canada	Klondike, Yukon Territory	-	-	160	[32]
<b>Samdong, Korea</b>	Youngdong mining district, Korea	4.2	<b>132.4</b>	Jurassic	[33]
Barneys Canyon, USA	Utah	0.45	14	147–159	[34]
Mouse Pass, USA	Alaska	-	-	95–110	[35]
Nuka Bay, USA	Alaska	-	-	95–110	[35]
Chichago mine, USA	Alaska	-	-	95–110	[35]
Berners Bay, USA	Alaska	-	-	95–110	[35]
Alaska-Juneau mine, USA	Alaska	-	-	95–110	[35]
Treadwell mine, USA	Alaska	-	-	95–110	[35]
Sumdum Chief mine, USA	Alaska	-	-	95–110	[35]
Willow Creek, USA	Alaska	-	-	95–110	[35]
Valdez Creek, USA	Alaska	-	-	95–110	[35]
Fairbanks, USA	Alaska	-	-	95–110	[35]
Ryan Lode, USA	Alaska	-	-	95–110	[35]
Fort Knox, USA	Alaska	1.4	45	95–110	[35]
Table Mountain, USA	Alaska	-	-	95–110	[35]
Rock Creek, USA	Alaska	-	-	95–110	[35]
Chandalar, USA	Alaska	-	-	95–110	[35]
<b>Dongping, China</b>	Hebei province	>3.2	<b>&gt;100</b>	153	[36]
Niuxinshan, China	E. Hebei, NE China	0.6	20	166	[37]
Hanshan, China	NW China	1.9	60	214–224	[38]
<b>Kyuchye, Russia</b>	Sakha-Yakutia	5	<b>157</b>	Late Cretaceous	[39]
Svetloye, Russia	Sakha-Yakutia	-	-	Mesozoic	[39]
Tas-Uryakhskoye, Russia	Khabarovsk	1.3	40	Cretaceous	[39]
Baidi, China	China	-	-	75–140	[40]
Baqi, China	Youjiang basin China	0.3	10	182–206	[40]
Dongbeizhai, China	China	2.25	70	Middle Jurassic	[40]
Gaolong, China	China	0.8	25	182–206	[40]
Gedang, China	China	0.2	7	182–206	[40]
Jinya, China	South China platform	1	30	Cretaceous	[40]
Lannigou, China	South China platform	2.6	80	182–206	[40]
Mingshan, China		0.3	10	182–206	[40]
Shijia, China		0.3	10	75–140	[40]
Humboldt, USA	Northwestern Nevada	-	-	Cretaceous	[41]
Dun Glen, USA	Northwestern Nevada	-	-	Cretaceous	[41]
Santa Rose, USA	Northwestern Nevada	-	-	Cretaceous	[41]
Ten Mile, USA	Northwestern Nevada	-	-	Cretaceous	[41]
Eugene, USA	Northwestern Nevada	-	-	Cretaceous	[41]
Slumbering, USA	Northwestern Nevada	-	-	Cretaceous	[41]
Antelope, USA	Northwestern Nevada	-	-	Cretaceous	[41]
Trinity, USA	Northwestern Nevada	-	-	Cretaceous	[41]
Pine Forest, USA	Northwestern Nevada	-	-	Cretaceous	[41]
Pueblo, USA	Northwestern Nevada	-	-	Cretaceous	[41]
Jackson, USA	Northwestern Nevada	-	-	Cretaceous	[41]
Quinn River, USA	Northwestern Nevada	-	-	Cretaceous	[41]
Wangu, China	Hunan province	0.4	13	70	[42]
Kuzhubao and Bashishan China	Yunnan Province, Fu Ning district	-	-	Mesozoic?	[43]
<b>Sanshandao, China</b>	North China platform, Jiaodong province	3.4	<b>107</b>	Early Cretaceous	[44]
<b>Dongping, China</b>	Hebei province,	3.2	<b>100</b>	153	[45]
<b>Donlin Creek, USA</b>	Northern Alaska	24.7	<b>770</b>	70	[46]
<b>Mayskoye, Russia</b>	Chukchi peninsula	3.6	<b>114</b>	107–115	[47]
Anjiayingzi, China	North China Craton	1.1	35	Mesozoic	[48]
Paishanlou, China	North China Craton	1.3	40	124–126	[49]
Denggezhuang, China	Muru Gold Belt in Eastern Shandong	1.4	44	Mesozoic	[50]
<b>Gubong, Korea</b>	Cheongyang gold district, Cheonan metallogenetic province	4.8	<b>150</b>	Early Cretaceous	[51]
Rushan, China	Jiaodong Peninsula	>1	>30	117	[52]
Baijintazi, China	Daduhe field, Tibetan Plateau	0.04	1.2	Mesozoic	[53]
Heijintaizi, China	Daduhe field, Tibetan plateau	0.05	1.5	Mesozoic	[53]
<b>Nezhdaninskoye, Russia</b>	Sakha-Yakutia	3.6	<b>114</b>	115–124	[54]
Linglong, China	Shandong Province	4	<b>124</b>	Early Cretaceous	[55]

Table 1. Cont.

Deposition *, Country	Province	Gold Content, Moz (Million Ounces)	Gold Content, Metric Tons	Age, Ma	Reference
<b>Mezococic</b>					
Sarylakh, Russia	Sakha-Yakutia	1.3	40	124	[56]
Sentachan, Russia	Sakha-Yakutia	0.6	20	Early Cretaceous	[56]
Dyby, Russia	NE Russia	0.96	30	125	[57]
Ergelyakh 1, Russia	NE Russia	0.1	3	140–149	[57]
Ergelyakh 2, Russia	NE Russia	0.1	3	140–149	[57]
Ergelyakh 3, Russia	NE Russia	0.1	3	140–149	[57]
<b>Arkachan, Russia</b>	W. Verkhoyanye	3.2	100	Mesozoic	[57]
Kimpichenskoye Russia	W. Verkhoyanye	-	-	Mesozoic	[58]
<b>Arkachan, Russia</b>	W. Verkhoyanye	3.2	100	Mesozoic	[58]
<b>Natalkinskoye, Russia</b>	NE Russia	3.2	100	135	[59]
Rodionovskoye, Russia	NE Russia	0.06	2	Early Cretaceous	[60]
Shuiyindong, China	Guizhou, Youjiang basin	1.8	55	182–206	[61]
Yata, China	Guizhou, Youjiang basin, S. China	0.32	10	182–206	[61]
Samgwang, Korea	Korea	2.3	72	127	[62]
Sentachan, Russia	Sakha-Yakutia	0.6	20	Early Cretaceous	[63]
Sarylakh, Russia	Sakha-Yakutia	1.3	40	Early Cretaceous	[63]
Guodawa, Songweizi, Tonggoucheng and Xiaomiaoshan, China	Zhangbaling Tectonic belt	-	-	116–118	[64]
Shkolnoye, Russia	NE Russia	0.06	2	135	[65]
Badrak, Russia	Sakha-Yakutia	0.45	14	Mesozoic?	[66]
Pogromnoye, Russia	Transbaykalia	1.6	50	Late Jurassic	[67]
Wenyu, China	North China Platform	>3.2	>100	127	[68]
Banqi, China	Youjiang basin	0.32	10	182–206	[69]
Bojitian, China	Youjiang basin S. China	0.5	15	182–206	[69]
Lannigou, China	South China platform	2.5	80	182–206	[69]
Shuiyindong, China	Guizhou, Youjiang basin	1.8	55	182–206	[69]
Taipingdong, China	Youjiang basin	1.8	57	182–206	[69]
Yata, China	Guizhou, Youjiang basin, S. China	0.5	15	182–206	[69]
Zimudang, China	Youjiang basin, S. China	1.9	60	182–206	[69]
Yangzhaiyu, China	North China Craton	1.1	34	124–141	[70]
Qianhe, China	Xiong'ershan area, North China Craton	-	-	124–135	[71]
<b>Sanshandao, China</b>	Jiaodong Peninsula, Shandong province	3.4	107	Early Cretaceous	[72]
<b>Jinshan, China</b>	between the Yangtze and Cathaysia blocks, South China	3.4	107	Mesozoic?	[73]
Gatsuurt, Mongolia	North Khentei Gold Belt, Central N Mongolia	<1.6	<50?	178	[74]
Taipingdong, China	Huijiabao gold district, Yangtze craton	1.8	57	182–206	[75]
Zimudang, China	Huijiabao gold district, Yangtze craton	1.9	60	182–206	[75]
Shuiyindong, China	Huijiabao gold district, Yangtze craton	1.8	55	182–206	[75]
Bojitian, China	Huijiabao gold district, Yangtze craton	0.5	15	182–206	[75]
Wenyu, China	North China Platform	>3.2	>100	127	[76]
<b>Sanshandao, China</b>	Jiaodong gold province	3.4	107	117.6 ± 3	[77]
<b>Arkachan, Russia</b>	W. Verkhoyanye	3.2	100	Mesozoic	[78]
Canan area, Honduras	Lepagure District, Central America	-	-	Cretaceous–Early Tertiary	[79]
<b>Zhaishang, China</b>	Min-Li metallogenic belt, W Qinling Mountains	>9.6	>300	220	[80]
Qiangma, China	North China Craton	>0.6	>20	130	[81]
<b>Dongfeng, China</b>		5.1	158	125	[82]
Linglong, China		4	124	125	[82]
<b>Erdaogou, Xiaobeigou, China</b>	Jiapigou gold province, NE China	>3.2	>100	219–228	[83]
<b>Sanshandao, China</b>	Jiaodong gold province	3.4	107	117.6 ± 3	[84]
Anjiayingzi, China	North China Craton	1.1	35	Mesozoic	[85]
Nancha, China	S. Jilin Province, northeast China	0.6	20	Mesozoic	[86]
<b>Taishang, China</b>	Jiaodong Peninsula, eastern China	32	1000	150–165	[87]
Jinchangyu, China	North China Craton	1.6	50	219–233	[88]
Hetai, China	Hetai goldfield, Bay-Hangzhou Bay metallogenic belt	<0.32	<10	Mesozoic	[89]
Liyuan, China	Central North China Craton	<1	<30	125	[90]
Baolun, China	Hainan Province of South China	0.6	20	224–228	[91]
Gezhen, China	Hainan Province of South China	-	-	224–228	[91]
<b>Dongping, China</b>	Hebei province	>3.2	>100	153	[92]
Xiadian, China	Jiaodong Peninsula	0.5	14.6	120–126	[93]
<b>Luoshan, China</b>	Jiaodong peninsula	4.8	149	125	[94]
Fushan, China	Jiaodong peninsula	0.5	15	125	[94]
Bake, China	Jiangnan Orogenic Belt, Yangtze Block	-	-	130–144	[95]
Chanziping, China	Jiangnan Orogenic Belt, Yangtze Block	0.68	21	130–144	[95]
Dagaowu, China	Jiangnan Orogenic Belt, Yangtze Block	-	-	130–144	[95]
Fenshuiao, China	Jiangnan Orogenic Belt, Yangtze Block	-	-	130–144	[95]
Gaokeng, China	Jiangnan Orogenic Belt, Yangtze Block	-	-	130–144	[95]
Hamashi, China	Jiangnan Orogenic Belt, Yangtze Block	-	-	130–144	[95]
Huangjindong, China	Jiangnan Orogenic Belt, Yangtze Block	2.6	80	130–144	[95]
Huangshan, China	Jiangnan Orogenic Belt, Yangtze Block	0.96	30	130–144	[95]

Table 1. Cont.

Deposition *, Country	Province	Gold Content, Moz (Million Ounces)	Gold Content, Metric Tons	Age, Ma	Reference
<b>Mezozoic</b>					
Huangtudian, China	Jiangnan Orogenic Belt, Yangtze Block	-	-	130–144	[95]
<b>Jinshan, China</b>	Jiangnan Orogenic Belt, Yangtze Block	9.6	<b>300</b>	130–144	[95]
Kengtou, China	Jiangnan Orogenic Belt, Yangtze Block	-	-	130–144	[95]
Miaoxiafan, China	Jiangnan Orogenic Belt, Yangtze Block	-	-	130–144	[95]
Mobin, China	Jiangnan Orogenic Belt, Yangtze Block	-	-	130–144	[95]
Pingshui, China	Jiangnan Orogenic Belt, Yangtze Block	-	-	130–144	[95]
Taojinchong, China	Jiangnan Orogenic Belt, Yangtze Block	-	-	130–144	[95]
Tonggu, China	Jiangnan Orogenic Belt, Yangtze Block	-	-	130–144	[95]
Tongshulin, China	Jiangnan Orogenic Belt, Yangtze Block	-	-	130–144	[95]
Wangu, China	Jiangnan Orogenic Belt, Yangtze Block	2.7	85	130–144	[95]
Xi'an, China	Jiangnan Orogenic Belt, Yangtze Block	-	-	130–144	[95]
Xichong, China	Jiangnan Orogenic Belt, Yangtze Block	-	-	130–144	[95]
Xintang, China	Jiangnan Orogenic Belt, Yangtze Block	-	-	130–144	[95]
Yanghanwu, China	Jiangnan Orogenic Belt, Yangtze Block	-	-	130–144	[95]
<b>Paleozoic</b>					
Hill End goldfield, Australia	New S. Wales	1.8	56	Early Carboniferous?	[96]
Haut Allier, France	Massif Central	<0.16	<5	260	[97]
Kvartsytoyev gorki, Kazakhstan	N. Kazakhstan	0.3	10	Late Ordovician?	[98]
<b>Zholymbet, Kazakhstan</b>	NW. Kazakhstan	7.7	<b>240</b>	Late Ordovician?	[98]
Bestobe, Kazakhstan	NW. Kazakhstan	9.6	<b>300</b>	Late Ordovician?	[98]
N. Aksu, Kazakhstan	NW. Kazakhstan	0.16	5	Late Ordovician?	[98]
S. Aksu, Kazakhstan	NW. Kazakhstan	14.5	<b>450</b>	Late Ordovician?	[98]
Stepnyak, Kazakhstan	NW. Kazakhstan	0.3	10	Late Ordovician?	[98]
Zhana-Tyube, Kazakhstan	NW. Kazakhstan	0.3	10	Late Ordovician?	[98]
Flying Pig, Australia	Hodgkinson field	0.02	0.5	Carboniferous	[99]
Tyrconnel, Australia	Hodgkinson field	0.06	2	Carboniferous	[99]
Pataz district, Peru		0.022	0.5?	305–321	[100]
Saralinskoye, Russia	Kuznetsk Alatau	0.7	22	Early to Late Silurian	[101]
Nagambie, Australia	Victoria	0.2	7	Silurian-Early Devonian	[102]
Kommunar, Russia	Kuznetsk Alatau	1.6	49	Silurian	[103]
<b>Zarmitan, Uzbekistan</b>	South Tien Shan	16	<b>500</b>	Syn- to post-Late Carboniferous	[104]
Central and North Deborah, Australia		0.2	7	Late Ordovician-middle Silurian	[105]
<b>Sukhoy log, Russia</b>	Bodaybo	48	<b>1500</b>	Paleozoic	[106]
<b>Berezovskoye, Russia</b>	Ural	15	<b>466</b>	Early Silurian	[107]
Fosterville, Australia	Victoria	0.16	5	Devonian	[108]
Vorontsovskoye, Russia	Ural	2.2	68	Late Devonian to Late Carboniferous	[39]
Biards district, France	Massif Central	0.13	4	300–305	[109]
Mayskoye, Russia	N. Karelia	<0.03	<1	397 ± 15	[110]
CSA Cobar, Australia	Cobar	2.6	83	Devonian	[111]
Moulin de Cheni, France	Saint-Yrieix district Massif Central	0.8	24	338	[112]
Jiapigou, China	S. Jilin Province,	1.9	60	Paleozoic?	[113]
Bulong, China	Akqi County, Southwest Tianshan	0.03	1	258	[114]
<b>Charters Tauers goldfield, Australia</b>	Tasman Fold Belt, Quinsleend	6.6	<b>207</b>	Early Devonian?	[115]
Sarekoubou, China	southern Altai, Xinjiang	<0.16	<5	320.6 ± 4	[116]
Qingshui, China	N. Xinjiang	<0.16	<5	315 ± 18	[117]
Tanjiānshan, China	W. China	2.3	73.9	269–288	[118]
Sandwich Point, Canada	Sandwich Point Meguma Terrane, Nova Scotia	0.05	1.6	380	[119]
Fosterville, Australia	Victoria	0.16	5	Devonian	[120]
Maldon, Australia	Victoria	1.8	56	445	[120]
<b>Stawell-Magdala, Australia</b>	Victoria	3.3	<b>105</b>	Ordovician	[120]
<b>Bendigo, Australia</b>	Victoria	17.1	<b>533</b>	Ordovician-Silurian	[120]
Wattle Gully, Australia	Victoria	0.4	12.9	Ordovician	[120]
Mount Piper, Australia	Victoria	<0.16	<5	Devonian	[120]
Woods Point, Australia	Victoria	0.9	28	Devonian	[120]
Walhalla (Cohen's Reef), Australia	Victoria	1.5	46	Devonian	[120]
Bogunayskoye, Russia	Enisey ridge	1.9	59	Paleozoic?	[121]
Annage, China	Qinghai Province, Kunlun orogenic belt	<0.16	<5	Paleozoic?	[122]
Woxi, China	Hunan Province	1.35	42	Paleozoic	[123]
Huangshan, China	Jiangshan-Shaoxing fault zone, South China	0.3	10	397 ± 34	[124]
Yingchengzi, China	Southern Heilongjiang Province, NE China	<0.16	<5	434–472	[125]
Limarinho, Portugal	northern Portugal, Variscan Iberian Massif	<0.16	<5	310–315	[126]
<b>Vasil'kovskoe, Kazakhstan</b>		12.2	<b>380</b>	312–279	[127]
Woxi, China	Hunan Province, Jiangnan Orogenic Belt, Yangtze Block	>1.3	>40	Paleozoic	[95]
<b>Sukoy Log, Russia</b>	Baikal-Patom	48	<b>1500</b>	Paleozoic	[128]
<b>Verninskoye, Russia</b>	Baikal-Patom	5.8	<b>180</b>	Paleozoic	[128]
Dogaldyn, Russia	Baikal-Patom	0.6	18	Paleozoic	[128]
Uryakh, Russia	Baikal-Muya	1.8	56	Paleozoic	[128]
Irokinda, Russia	Baikal-Muya	1.9	60	Paleozoic	[128]

Table 1. Cont.

Deposition *, Country	Province	Gold Content, Moz (Million Ounces)	Gold Content, Metric Tons	Age, Ma	Reference
<b>Meso- and Neoproterozoic</b>					
Olimpiadinskoye, Russia	Yenisey fold belt	11.7	365	594	[129]
Cachoeira de Minas, São Francisco, Brazil	Borborema Province	<0.3	<10	750	[130]
Veduga, Russia	Yenisey fold belt	4.8	149	600	[131]
Olimpiadinskoye, Russia	Yenisey fold belt	11.7	365	594	[131]
Harnas area, Sweden	Grenville province	0.03	1	1200	[132]
Paiol mine, Brazil	Almas Greenstone Belt, Tocantins State	0.6	18	535–702	[133]
Udereyskoye, Russia	Enisey Ridge	0.5	14.7	Proterozoic	[56]
Tunkillia, Nuckulla Hill, Barns, and Weednanna, Australia	Central Gawler Craton	0.7	22	1567–1596	[134]
Tarcoola gold field, S. Australia	Central Gawler Craton	0.7	22.7	1580	[135]
Telfer, Australia	Pilbara	19.0	591	590–640	[136]
<b>Paleoproterozoic</b>					
Tartan Lake, Canada	N. Manitoba	0.1	3	1791	[137]
Star Lake, Canada	La Ronge region, Northern Saskatchewan	0.12	3.9	1848	[138]
Flin Flon Domain, Canada	Trans-Hudson orogeny, Saskatchewan	0.6	19	1791	[139]
Pirila, Finland	Scandinavian	0.04	1.2	1810–1830	[140]
Star Lake (La Ronge), Canada	La Ronge region, Northern Saskatchewan	0.37	11.5	1848	[141]
Caxias, Brazil	Sao Luis craton	0.03	1	1990–2009	[142]
Fazenda Canto, Brazil	Sao Francisco craton, state of Bahia	0.3	10	1800–2200	[143]
Fazenda Maria Preta, Brazil	Sao Francisco craton, state of Bahia	0.5	15	1800–2200	[143]
Fazenda Brasileiro, Brazil	Sao Francisco craton, state of Bahia	2.2	70	1800–2200	[143]
Guarim, Brazil	Tapajos province	<0.3	<10	1880	[144]
Batman, Australia	Burrell Creek Formation	0.3	10	1800–1835	[145]
Serrinha, Brazil	Granite-Related	0.5	15.1	2160	[146]
Callie, Australia	Dead Bullock Soak goldfield	5.8	180	1815–1825	[147]
Coyote Prospect, Australia	Killi Killi Formation	0.45	14	1790–1840	[147]
Groudrust, Australia	Granites goldfield	0.7	22.7	1790–1840	[147]
Tanami gold field, Australia	Mount Charles Formation	1.6	50.9	1790–1840	[147]
Angovia, W. Africa	the Yaoure' area of central Ivory Coast in the West African craton	0.3	10	2050–2250	[148]
Chega Tudo, Brazil	the Gurupi belt of northern Brazil	1.9	60	2000	[149]
Bjorkdal, Sweden	Skellefte District, Northern Sweden	0.6	20	1780–1790	[150]
Carara, Brazil	Guiana Shield	0.3	10	2030	[151]
Morila, Mali	The Birimian schist belts of West Africa	7.0	217	2095–2103	[152]
Loulou 3, Mali	Loulou mining district, Mali, West Africa	1.0	32	Proterozoic	[153]
Gara, Mali	Loulou mining district, Mali, West Africa	3.1	97	Proterozoic	[153]
Yalea, Mali	Loulou mining district, Mali, West Africa	6.3	195	Proterozoic	[153]
Gounkoto, Mali	Loulou mining district, Mali, West Africa	-	-	Proterozoic	[153]
Piaba, Brasil	São Luís cratonic fragment	3.9	120	2170–2240	[154]
Turmalina, Brazil	Pitangui Shear Zone, Quadrilátero Ferrífero	1.2	37	1750	[155]
Piaba, Brasil	São Luís cratonic fragment	3.5	109	2227–2240	[156]
Julie, Ghana	The Leo Man Craton in West Africa	1.0	31	1980–2130	[157]
Lamego, Brazil	Rio das Velhas greenstone belt, Quadrilátero Ferrífero	0.4	13	2041	[158]
<b>Meso-Neoarchean</b>					
Henderson, Canada	Superior	1.3	42	Late Arhaean	[159]
McInture-Hollinger, Canada	Superior, Timmins	31.7	987	2673–2690	[160]
Kolar, India	Dharwar craton	26.9	838	Late Arhaean	[161]
Renabie, Canada	Wawa belt, Superior	1.3	40	2722–2728	[162]
Mink Lake, Canada	Superior	<0.03	<1	2730	[163]
Sigma, Canada	Superior	11.5	358	2705	[164]
Kolar, India	Dharwar craton	26.9	838	Late Arhaean	[165]
Pamour, Canada	Superior	7.9	247	2703–2725	[166]
Abbots, South Africa	Barberton	0.004	0.12	3084–3126	[167]
Bellevue, South Africa	Barberton	0.01	0.3	3084–3126	[167]
Pioneer, South Africa	Barberton	0.15	4.55	3084–3126	[167]
Surluga, Canada	Superior	12.4	385	2744	[168]
Sigma, Canada	Superior	11.5	358	2705	[169]
Donaldda, Canada	Superior	<1.0	<30	Arhaean	[169]
Dumont, Canada	Superior	<0.3	<10	Arhaean	[169]
Champion Iode, Nundydroog, Kolar, India	Dharwar craton	25.5	794	Late Archaean	[170]
Wiluna, Australia	Yilgarn Block	8.5	265	Archean	[171]
Bronzewing, Australia	Yilgarn Block	2.7	84	Archean	[172]
Siscoe, Canada	Superior Abitibi, Ontario	0.9	27	Late Archean	[173]
Junction, Australia	Yilgarn Block	6.7	209	Archean	[174]
Golden Eagle, Australia	Mosquito Creek belt, Pilbara Craton	0.4	13.1	2850–2900	[175]
Orenada 2, Cadillac tectonic zone, Canada	Superior	<1.0	<30	2682–2691	[176]
Hutti, India	Dharwar craton	17.1	533	2510–2750	[177]
Golden Crown, Australia	Murchison province, Yilgarn Block	1.1	33.5	2600–2800	[178]
Wiluna, Australia	Wiluna greenstone belt, Yilgarn Block	8.5	265	2749	[179]

**Table 1.** *Cont.*

Deposition *, Country	Province	Gold Content, Moz (Million Ounces)	Gold Content, Metric Tons	Age, Ma	Reference
<b>Meso-Neoarchean</b>					
Ramepuro, Finland	Ilomantsi greenstone belt, Scandinavian province	0.04	1.25	2700–2750	[180]
<b>Woodcutters field, Australia</b>	Kalgoorlie district, Yilgarn Block	38.6	<b>1200</b>	Archaean	[181]
McPhee, Australia	Pilbara Craton	<0.3	<10	2890–2950	[182]
Tarmoola, Australia	Yilgarn Block	3.7	<b>116</b>	2620–2780	[183]
Mount Charlotte, Australia	Yilgarn Block, Kalgoorlie	4.0	<b>125</b>	Archaean	[184]
Giant, Canada	Slave, Yellowknife greenstone belt	7.9	<b>246</b>	2660–2820	[185]
Uti, India	Dharwar craton	12.9	<b>400</b>	2576	[186]
Primrose, Zimbabwe	Kwekwe district, Midlands greenstone belt, Zimbabwe craton	0.14	4.3	2600–2650	[187]
Jojo, Zimbabwe	Kwekwe district Midlands greenstone belt, Zimbabwe craton	0.02	0.5	2600–2650	[187]
Indarama, Zimbabwe	Kwekwe district Midlands greenstone belt, Zimbabwe craton	0.16	5.1	2600–2650	[187]
Hutti, India	Hutti-Maski greenstone belt, Dharwar craton	>3.2	<b>&gt;100</b>	2532	[188]
Hira-Buddini, India	Hutti-Maski greenstone belt, Dharwar craton	6.4	<b>200</b>	2532	[188]
Sunrise Dam, Australia	Yilgarn Block	1.2	36.7	2670	[189]
Missouri, Australia	Yilgarn Block	0.03	0.9	Archaean	[190]
Klipwal Gold Mine, South Africa	Klipwal Shear Zone, SE Kaapvaal Craton,	0.5	15	2863–2721	[191]

Notes: \* In Tables 1–7, deposits printed in bold face have gold reserves of 100 tonnes or more.

### 3. Characteristics of the Mineralizing Fluids

This section is devoted to characteristics of the fluid regime under which gold deposits of various age groups were formed, with the deposits discussed from youngest to oldest. For each group of deposits, we report the state of the fluids (homogeneous or heterogeneous), brief characteristics of their phases ( $\text{H}_2\text{O}$ –salt solution, dense gas), and the principal parameters of the fluid inclusions (homogenization temperatures, salinity, and fluid trapping pressure).

#### 3.1. Cenozoic Deposits

Characteristics of mineral-forming fluids are presented in Table 2 and shown in Figures 1–5. The information includes 308 temperature and fluid salinity estimates and 106 pressure estimates. Some of these deposits were produced from homogeneously trapped aqueous-carbonic and generally low-salinity fluids that show no discernible evidence of unmixing (Zhemulang, Mazhala, and Bangbu, China; Muteh, Iran; and Zopkhito, Georgia Republic). However, most of these deposits were formed by heterogeneously trapped fluids, with one end-member being an aqueous-saline solution and the other being a high-density gas mixture dominated by  $\text{CO}_2$ . The trapping temperatures for the fluids range from 128 to 424 °C (median 242 °C) and salinities range from 0.0 to 19.6 wt.% NaCl equiv. (median 3.6 wt.% NaCl equiv.) (Table 8). The fluid trapping pressures vary from 150 to 3600 bar (median 1305 bar). The aqueous-only fluid (not related to fluid unmixing) without traces of fluid heterogenization showed lower homogenization temperatures (146–390 °C) and slightly higher salinities (0.5–19.6 wt.% NaCl equiv) than those of the aqueous phase of the heterogeneous fluids (temperature of 128–124 °C, salinity 0.0–14.6 wt.% NaCl equiv).

#### 3.2. Mesozoic Deposits

Data for mineral-forming fluids are summarized in Table 3 and portrayed in Figures 1–5. The information of the deposits comprises 1478 temperature and fluid salinity estimates and 440 pressure estimates. Some of these deposits were formed by homogeneously aqueous-carbonic fluid without evidence of unmixing. These include Big Hurrah, Willow Creek, Fairbanks, Table Mountain, and Donlin Creek, Alaska, USA; Yata, Dongping, Hanshan, Baidi, Banqi, Dongbeizhai, Gaolong, Gedang, Jinya, Lannigou, Mingshan, Shijia, Wangu, Kuzhubao, Bashishan, Anjiayingzi, Denggezhuang, Rushan, Baijintazi, Heijintaizi, Linglong, Shuiyindong, Guodawa, Songweizi, Tonggoucheng, Xiaomiaoshan, Bojitian, Lannigou, Taipingdong, Zimudang, Qianhe, Erdaogou, Xiaobeigou, Taishang, Jinchangyu,

Gezen, Hamashi, Pingshui, and Tonggu, China; Daeil and Samgwang, Korea; Lover Dominion and Portland Creek, Canada; Kyuchus, Svetloye, Tas-Uryakhskoye, and Kimpichenskoye, Russia; Gatsuurt, Mongolia; and Canan area, Honduras. The majority of deposits, however, trapped heterogeneous fluids below the appropriate solvi, with unmixing of H<sub>2</sub>O- and CO<sub>2</sub>-dominant fluid endmembers. Ore-forming fluids had temperatures of 80–515 °C (median 260 °C), salinities of 0.0 to 37.5 wt.% NaCl equiv. (median 5.9 wt.% NaCl equiv.), and pressures of 100 to 4000 bar (median 1200 bar) (Table 8). Just like the previous case, the pure aqueous fluids without traces of fluid heterogenization showed lower homogenization temperatures (80–421 °C) and slightly lower salinities (0.02–32.7 wt.% NaCl equiv) than those of the aqueous phase of the heterogeneous fluids (temperature of 92–515 °C, salinity 0.0–37.5 wt.% NaCl equiv).

**Table 2.** Parameters of mineralizing fluids of Cenozoic gold deposits.

Deposit, Region	Physicochemical Parameters of Fluids					Reference
	T, °C	Salinity *, wt.%	d, g/cm <sup>3</sup>	P, bar	Composition **	
Valdez Group, USA	210–280 (2)	0–6.0	-	1000–1500 (2)	CO <sub>2</sub> + H <sub>2</sub> O	[6]
Venus, Canada	231–316 (45)	1.8–5.4	-	250–2700 (37)	CO <sub>2</sub> + H <sub>2</sub> O	[7]
Monte Rosa gold district, Italy	180–330 (19)	1.0–10.1	0.86–0.93	1000–1500 (2)	CO <sub>2</sub> + H <sub>2</sub> O	[8]
Fairview, Oro Fino, Canada	275–313 (2)	2.7–4.7	0.73–0.78	800–1550 (7)	CO <sub>2</sub> + H <sub>2</sub> O	[9]
Twin Lakes Canada	270–323 (2)	1.2–8.6	0.77–0.78	-	H <sub>2</sub> O	[9]
<b>Alaska-Juneau, USA</b>	150–300 (2)	0.0–5.0	-	1000–2000 (2)	CO <sub>2</sub> + H <sub>2</sub> O	[10]
Ibex, USA	150–300 (2)	0.0–5.0	-	1000–2000 (2)	CO <sub>2</sub> + H <sub>2</sub> O	[10]
Reagan, USA	150–280 (2)	0.0–5.0	-	1000–2000 (2)	CO <sub>2</sub> + H <sub>2</sub> O	[10]
Treadwell, USA	190–240 (2)	5.0–8.0	-	800–1500 (2)	H <sub>2</sub> O	[10]
<b>Bralorne-Pioneer, Canada</b>	140–350 (10)	0.8–5.0	-	500–1750 (4)	CO <sub>2</sub> + H <sub>2</sub> O	[11]
Monte Rosa gold district, Italy	230–300 (2)	1.2–1.9	-	600–1300 (2)	CO <sub>2</sub> + H <sub>2</sub> O	[12]
<b>Bralorne-Pioneer, Canada</b>	150–390 (36)	0.9–10.5	0.62–0.93	-	H <sub>2</sub> O	[13]
Callery, New Zealand	300–350 (2)	2.0	-	900–1200 (2)	CO <sub>2</sub> + H <sub>2</sub> O	[14]
Shotover, New Zealand	160–200 (2)	0.5	-	500–1000 (2)	CO <sub>2</sub> + H <sub>2</sub> O	[14]
Mt. Alta, New Zealand	160–260 (2)	2.0	-	500–1000 (2)	CO <sub>2</sub> + H <sub>2</sub> O	[14]
Nenthorn, New Zealand	190 (1)	2.0	-	150 (1)	CO <sub>2</sub> + H <sub>2</sub> O	[14]
Böckstein, Austria	240–270 (8)	5	-	700 (1)	CO <sub>2</sub> + H <sub>2</sub> O	[15]
Monte Rosa gold district, Italy	250–300 (4)	5	-	1000 (1)	CO <sub>2</sub> + H <sub>2</sub> O	[15]
Kensington, USA	170–220 (2)	5.0–8.0	-	900 (2)	CO <sub>2</sub> + H <sub>2</sub> O	[16]
Jualin, USA	170–220 (2)	6.5–9.0	-	900 (2)	CO <sub>2</sub> + H <sub>2</sub> O	[16]
Shannan area, China	232–335 (4)	4.0–15.0	0.68–0.95	-	H <sub>2</sub> O	[17]
Muteh, Iran	156–305 (4)	2.2–17.5	-	-	CO <sub>2</sub> + H <sub>2</sub> O	[18]
Zopkhito, Georgia Republic	185–380 (53)	0.5–4.9	0.52–0.91	-	H <sub>2</sub> O	[19]
<b>La Herradura, Mexico</b>	265–283 (7)	3.5–4.1	-	670–2015 (7)	CO <sub>2</sub> + H <sub>2</sub> O	[20]
Daping, China	279–424 (8)	3.7–14.6	0.69–0.78	1335–3400 (2)	CO <sub>2</sub> + H <sub>2</sub> O	[21]
Mayum, China	229–357 (19)	1.2–5.8	0.65–0.84	1400–3500 (18)	CO <sub>2</sub> + H <sub>2</sub> O	[22]
Zhemulang, China	146–292 (24)	3.2–7.7	0.79–0.96	-	H <sub>2</sub> O	[23]
Mazhalia, China	148–303 (30)	1.6–5.1	0.75–0.94	-	H <sub>2</sub> O	[23]
Qolqoleh, Iran	204–386 (6)	4.9–19.6	-	1600–2000 (2)	CO <sub>2</sub> + H <sub>2</sub> O	[24]
Bangbu, China	167–336 (6)	2.2–9.5	0.63–0.96	-	H <sub>2</sub> O	[25]

Notes: \* salinity of fluid expressed in wt% NaCl equiv.; \*\* composition of gas phase of fluid inclusions; Number of determinations is shown in parentheses.

**Table 3.** Parameters of mineralizing fluids of Mesozoic gold deposits.

Deposit, Region	Physicochemical Parameters of Fluids					Reference
	T, °C	Salinity *, wt.%	d, g/cm <sup>3</sup>	P, bar	Composition **	
Oriental mine, USA	280–340 (2)	0.0–3.5	—	670–2500	CO <sub>2</sub> + H <sub>2</sub> O	[26]
Big Hurrah mine, USA	155–240 (9)	2.2–6.8	0.88–0.95	—	H <sub>2</sub> O	[27]
Mouther Lode, USA	290–350 (2)	2.0	—	1000–2000	CO <sub>2</sub> + H <sub>2</sub> O	[28]
Yata, China	150–240 (2)	5.0	0.86–0.96	—	H <sub>2</sub> O	[29]
Daeil, Korea	243–375 (4)	3.1–9.1	0.56–0.89	—	H <sub>2</sub> O	[30]
Macraes, New Zealand	300–350 (2)	1.0	—	2500–3500	CO <sub>2</sub> + H <sub>2</sub> O	[14]
Glenorchy, New Zealand	200–300 (2)	1.0	—	2000	CO <sub>2</sub> + H <sub>2</sub> O	[14]
Barewood, New Zealand	300	1.0–2.0	—	2000	CO <sub>2</sub> + H <sub>2</sub> O	[14]
Bendigo, New Zealand	<290	1.9	—	>1000	CO <sub>2</sub> + H <sub>2</sub> O	[14]
Bonanza, New Zealand	200	1.5	—	800–1400	CO <sub>2</sub> + H <sub>2</sub> O	[14]
Quartz Hill, USA	375 (1)	6.0	—	1350	CO <sub>2</sub> + H <sub>2</sub> O	[31]
Lover Dominion, Canada	296 (1)	3.4	—	—	H <sub>2</sub> O	[32]
Aime, Canada	263 (1)	4.9	—	2300 (1)	CO <sub>2</sub> + H <sub>2</sub> O	[32]
Gold Run, Canada	278–293 (2)	4.0–4.3	—	1325–1500 (2)	CO <sub>2</sub> + H <sub>2</sub> O	[32]
Portland Creek, Canada	255 (1)	4.0	—	—	H <sub>2</sub> O	[32]
Lloyd, Canada	304–308 (2)	3.8–4.3	—	870–1440 (2)	CO <sub>2</sub> + H <sub>2</sub> O	[32]
Hunker Dome, Canada	310–332 (2)	4.0–5.0	—	750–1250 (2)	CO <sub>2</sub> + H <sub>2</sub> O	[32]
Mitchell, Canada	296–341 (4)	2.4–6.1	—	450–875 (4)	CO <sub>2</sub> + H <sub>2</sub> O	[32]
Sheba, Canada	281–341 (6)	2.9–6.8	—	450–1800 (6)	CO <sub>2</sub> + H <sub>2</sub> O	[32]
Lone Star, Canada	292 (1)	3.2	—	300	CO <sub>2</sub> + H <sub>2</sub> O	[32]
Hilchey, Canada	297 (1)	5.8	—	300	CO <sub>2</sub> + H <sub>2</sub> O	[32]
27 Pup, Canada	313 (1)	3.5	—	300	CO <sub>2</sub> + H <sub>2</sub> O	[32]
Violet, Canada	225 (1)	6.1	—	350	CO <sub>2</sub> + H <sub>2</sub> O	[32]
Virgin, Canada	198 (1)	5.5	—	625	CO <sub>2</sub> + H <sub>2</sub> O	[32]
Amethyst, Canada	341 (1)	1.2	—	350	CO <sub>2</sub> + H <sub>2</sub> O	[32]
<b>Samdong, Korea</b>	102–426 (24)	2.7–14.0	0.88–0.94	1300–1900 (2)	CO <sub>2</sub> + H <sub>2</sub> O	[33]
Barneys Canyon, USA	225–345 (2)	1.5	0.60–0.85	—	H <sub>2</sub> O	[34]
Mouse Pass, USA	210–360	1.0–3.0	—	1000–1500	CO <sub>2</sub> + H <sub>2</sub> O	[35]
Nuka Bay, USA	250–300	3.0–6.0	—	2300–3000	CO <sub>2</sub> + H <sub>2</sub> O	[35]
Chichagof mine, USA	225–250	6.0	—	1000	CO <sub>2</sub> + H <sub>2</sub> O	[35]
Berners Bay, USA	200–235	3.0–6.0	—	900	CO <sub>2</sub> + H <sub>2</sub> O	[35]
Alaska-Juneau mine, USA	300–375	0.0–5.0	—	1500–4000	CO <sub>2</sub> + H <sub>2</sub> O	[35]
Treadwell mine, USA	190–240	0.0–5.0	—	800–1500	CO <sub>2</sub> + H <sub>2</sub> O	[35]

Table 3. Cont.

Deposit, Region	Physicochemical Parameters of Fluids					Reference
	T, °C	Salinity *, wt.%	d, g/cm <sup>3</sup>	P, bar	Composition **	
Sumdum Chief mine, USA	240–320	0.0–5.0	-	800–1500	CO <sub>2</sub> + H <sub>2</sub> O	[35]
Willow Creek, USA	300–325	1.0–2.5	-	-	H <sub>2</sub> O	[35]
Valdez Creek, USA	290–305	-	-	1000–2300	CO <sub>2</sub> + H <sub>2</sub> O	[35]
Fairbanks, USA	275–375	3.0–5.0	-	-	H <sub>2</sub> O	[35]
Ryan Lode, USA	270–350	0.0–8.0	-	500–750	CO <sub>2</sub> + H <sub>2</sub> O	[35]
Fort Knox, USA	270–330	0.0–8.0	-	1250–1500	CO <sub>2</sub> + H <sub>2</sub> O	[35]
Table Mountain, USA	320–370	3.0–7.0	-	-	H <sub>2</sub> O	[35]
Rock Creek, USA	184–272	5.0	-	1000–1400	CO <sub>2</sub> + H <sub>2</sub> O	[35]
Chandalar, USA	265–300	0.8–3.0	-	750–825	CO <sub>2</sub> + H <sub>2</sub> O	[35]
<b>Dongping, China</b>	195–340 (4)	2.5–21.0	0.64–1.04	-	H <sub>2</sub> O	[36]
Niuxinshan, China	180–336 (11)	4.1–9.6	0.77–0.92	750–3700 (9)	CO <sub>2</sub> + H <sub>2</sub> O	[37]
Hanshan, China	150–310 (5)	3.1–10.7	0.72–0.95	-	H <sub>2</sub> O	[38]
<b>Kyuchus, Russia</b>	118 (1)	2.8	0.97	-	H <sub>2</sub> O	[39]
Svetloye, Russia	145–215 (4)	6.4–14.0	0.90–1.02	-	H <sub>2</sub> O	[39]
Tas-Uryakhskoye, Russia	155 (1)	2.0	0.93	-	H <sub>2</sub> O	[39]
Baidi, China	172–266 (5)	3.9–6.6	0.84–0.93	-	H <sub>2</sub> O	[40]
Banqi, China	180–230 (2)	3.2	0.86–0.91	-	H <sub>2</sub> O	[40]
Dongbeizhai, China	120–170 (2)	5.0	0.94–0.98	-	H <sub>2</sub> O	[40]
Gaolong, China	125–290 (5)	2.4–5.1	0.78–0.96	-	H <sub>2</sub> O	[40]
Gedang, China	155–305 (4)	3.4–6.0	0.77–0.94	-	H <sub>2</sub> O	[40]
Jinya, China	143–270 (4)	2.9–5.1	0.82–0.95	-	H <sub>2</sub> O	[40]
Lannigou, China	160–253 (3)	4.5–4.9	0.84–0.95	-	H <sub>2</sub> O	[40]
Mingshan, China	136–185 (2)	4.0–5.0	0.92–0.96	-	H <sub>2</sub> O	[40]
Shijia, China	152–225 (3)	1.9–6.7	0.87–0.93	-	H <sub>2</sub> O	[40]
Humboldt, USA	170–340 (12)	0.2–11.2	-	1200–2400 (2)	CO <sub>2</sub> + H <sub>2</sub> O	[41]
Dun Glen, USA	150–260 (4)	1.0–8.8	-	1200–2400 (2)	CO <sub>2</sub> + H <sub>2</sub> O	[41]
Santa Rose, USA	200–360 (12)	0.2–8.3	-	1200–2400 (2)	CO <sub>2</sub> + H <sub>2</sub> O	[41]
Ten Mile, USA	240–350 (2)	1.0–7.9	-	1200–2400 (2)	CO <sub>2</sub> + H <sub>2</sub> O	[41]
Eugene, USA	170–330 (12)	0.2–9.5	-	1200–2400 (2)	CO <sub>2</sub> + H <sub>2</sub> O	[41]
Slumbering, USA	180–330 (8)	0.4–10.4	-	1200–2400 (2)	CO <sub>2</sub> + H <sub>2</sub> O	[41]
Antelope, USA	180–340 (8)	0.2–8.4	-	1200–2400 (2)	CO <sub>2</sub> + H <sub>2</sub> O	[41]
Trinity, USA	195–300 (4)	1.0–9.9	-	1200–2400 (2)	CO <sub>2</sub> + H <sub>2</sub> O	[41]
Pine Forest, USA	220–330 (8)	0.4–16.7	-	1200–2400 (2)	CO <sub>2</sub> + H <sub>2</sub> O	[41]
Pueblo, USA	250–350 (4)	0.8–17.5	-	1200–2400 (2)	CO <sub>2</sub> + H <sub>2</sub> O	[41]

Table 3. Cont.

Deposit, Region	Physicochemical Parameters of Fluids					Reference
	T, °C	Salinity *, wt.%	d, g/cm <sup>3</sup>	P, bar	Composition **	
Jackson, USA	100–230 (2)	6.7–15.3	-	1200–2400 (2)	CO <sub>2</sub> + H <sub>2</sub> O	[41]
Quinn River, USA	170–330 (4)	1.8–20.0	-	1200–2400 (2)	CO <sub>2</sub> + H <sub>2</sub> O	[41]
Wangu, China	138–310 (14)	3.0–6.0	0.73–0.97	-	H <sub>2</sub> O	[42]
Kuzhubao and Bashishan, China	180–330 (8)	0.8–13.0	0.77–0.90	-	H <sub>2</sub> O	[43]
Sanshandao, China	150–355 (35)	1.5–7.1	0.62–0.95	1200–2100 (46)	CO <sub>2</sub> + H <sub>2</sub> O	[44]
Dongping, China	250–372 (33)	4.7–8.9	0.64–0.87	600–1800 (31)	CO <sub>2</sub> + H <sub>2</sub> O	[45]
Donlin Creek, USA	232–237 (2)	6.3	0.88	-	H <sub>2</sub> O	[46]
Mayskoye, Russia	119–515 (28)	0.9–37.5	0.57–1.13	420–1240 (28)	CO <sub>2</sub> + H <sub>2</sub> O	[47]
Anjiayingzi, China	160–338 (3)	2.0–4.5	-	-	CO <sub>2</sub> + H <sub>2</sub> O	[48]
Paishanlou, China	128–447 (14)	3.1–33.3	0.89–0.96	1400–1900 (2)	CO <sub>2</sub> + H <sub>2</sub> O	[49]
Denggezhuang, China	80–388 (45)	1.1–16.4	0.71–0.99	-	H <sub>2</sub> O	[50]
Gubong, Korea	201–432	0.4–17.3	-	670–2100	CO <sub>2</sub> + CH <sub>4</sub> + H <sub>2</sub> O	[51]
Rushan, China	96–324 (4)	0.2–12.6	0.80–1.04	-	CO <sub>2</sub> + H <sub>2</sub> O	[52]
Baijintazi, China	180–386 (10)	6.9–13.2	0.72–0.97	-	H <sub>2</sub> O	[53]
Heijintaizi, China	182–361 (15)	6.7–18.5	0.85–0.94	-	H <sub>2</sub> O	[53]
Nezhdaninskoye, Russia	129–378 (40)	0.8–31.1	0.65–1.12	390–1840 (33)	CO <sub>2</sub> + H <sub>2</sub> O	[54]
Linglong, China	80–360 (14)	3.0–14.6	0.60–1.00	-	H <sub>2</sub> O	[55]
Sarylakh, Russia	130–380 (3)	0.5–6.4	0.62–0.94	-	H <sub>2</sub> O	[56]
Sentachan, Russia	200–325 (2)	5.7	0.73–0.91	-	H <sub>2</sub> O	[56]
Dyby, Russia	226–495 (6)	6.9–35.3	0.86–0.91	477–1495 (4)	CO <sub>2</sub> + H <sub>2</sub> O	[57]
Ergelyakh 1, Russia	243–358 (5)	3.7–32.7	0.84–0.98	-	H <sub>2</sub> O	[57]
Ergelyakh 2, Russia	264–304 (4)	4.5–8.6	0.77–0.82	940–1140 (2)	CO <sub>2</sub> + H <sub>2</sub> O	[57]
Ergelyakh 3, Russia	268 (1)	3.6	0.80	-	H <sub>2</sub> O	[57]
Arkachan, Russia	250–385 (2)	3.7–26.3	0.83–0.89	1300–1700 (2)	CO <sub>2</sub> + H <sub>2</sub> O	[57]
Kimpichenskoye Russia	200 (1)	32.0	1.13	-	H <sub>2</sub> O	[58]
Arkachan, Russia	230–290 (4)	12.0–20.0	0.87–0.99	-	H <sub>2</sub> O	[58]
Natalkinskoye, Russia	205–359 (12)	1.9–6.2	0.60–0.91	1120–2260 (13)	CO <sub>2</sub> + H <sub>2</sub> O	[59]
Rodionovskoye, Russia	294–337 (2)	6.8–7.3	0.87–0.95	1180–1530 (2)	CO <sub>2</sub> + H <sub>2</sub> O	[60]
Shuiyindong, China	212–225 (2)	4.7–6.3	0.89	-	H <sub>2</sub> O	[61]
Yata, China	151–261 (9)	2.1–7.2	0.85–0.94	-	H <sub>2</sub> O	[61]
Samgwang, Korea	145–385 (13)	0.1–11.2	0.70–0.93	-	H <sub>2</sub> O	[62]
Sentachan, Russia	155–320 (11)	1.6–7.4	0.82–1.03	1310–1960 (13)	CO <sub>2</sub> + H <sub>2</sub> O	[63]
Sarylakh, Russia	170–312 (12)	1.6–6.8	0.89–1.06	300–3430 (17)	CO <sub>2</sub> + H <sub>2</sub> O	[63]

Table 3. Cont.

Deposit, Region	Physicochemical Parameters of Fluids					Reference
	T, °C	Salinity *, wt.%	d, g/cm <sup>3</sup>	P, bar	Composition **	
Guodawa, Songweizi, Tonggoucheng, and Xiaomiaoshan, China	115–335 (20)	5.6–11.6	0.72–1.02	-	H <sub>2</sub> O	[64]
Shkolnoye, Russia	189–350 (23)	2.1–9.3	0.77–1.03	365–2320 (8)	CO <sub>2</sub> + H <sub>2</sub> O	[65]
Badran, Russia	140–320 (3)	4.5–10	0.80–0.96	100–2000 (2)	CO <sub>2</sub> + H <sub>2</sub> O	[66]
Pogromnoye, Russia	283–363 (6)	6.5–11.1	0.81–1.02	980–2800 (11)	CO <sub>2</sub> + H <sub>2</sub> O	[67]
<b>Wenyu, China</b>	114–330 (12)	0.1–12.8	0.63–0.98	850–1780 (4)	CO <sub>2</sub> + H <sub>2</sub> O	[68]
Banqi, China	210–290 (2)	2.3–4.2	0.77–0.87	-	H <sub>2</sub> O	[69]
Bojitian, China	117–193 (3)	0.5–6.9	0.93–0.95	-	H <sub>2</sub> O	[69]
Lannigou, China	85–272 (8)	0.5–8.7	0.85–0.97	-	H <sub>2</sub> O	[69]
Shuiyindong, China	126–225 (5)	0.2–6.3	0.89–0.95	-	H <sub>2</sub> O	[69]
Taipingdong, China	172–269 (7)	1.9–7.3	0.84–0.94	-	H <sub>2</sub> O	[69]
Yata, China	106–231 (3)	0.7–7.9	0.90–0.96	-	H <sub>2</sub> O	[69]
Zimudang, China	95–273 (5)	0.2–7.5	0.84–0.97	-	H <sub>2</sub> O	[69]
Yangzhaiyu, China	175–313 (16)	5.1–13.6	0.78–0.99	-	CO <sub>2</sub> + H <sub>2</sub> O	[70]
Qianhe, China	160–305 (64)	6.1–21.8	0.93–0.95	-	H <sub>2</sub> O	[71]
<b>Sanshandao, China</b>	112–350 (12)	0.4–10.3	0.75–0.96	-	H <sub>2</sub> O	[72]
<b>Jinshan China</b>	109–340 (15)	0.6–8.9	0.70–0.96	-	H <sub>2</sub> O	[73]
Gatsuurt, Mongolia	194–355 (10)	-	-	-	CO <sub>2</sub> + H <sub>2</sub> O	[74]
Taipingdong, China	97–300 (8)	0.02–8.1	-	-	CO <sub>2</sub> + H <sub>2</sub> O	[75]
Zimudang, China	99–300 (6)	0.04–7.5	-	-	CO <sub>2</sub> + H <sub>2</sub> O	[75]
Shuiyindong, China	83–250 (8)	0.02–6.9	-	-	CO <sub>2</sub> + H <sub>2</sub> O	[75]
Bojitian, China	80–198 (2)	0.9–7.5	-	-	H <sub>2</sub> O	[75]
<b>Wenyu, China</b>	114–417 (36)	0.0–12.8	-	1570–2760 (6)	CO <sub>2</sub> + H <sub>2</sub> O	[76]
<b>Sanshandao, China</b>	101–390 (6)	0.2–18.4	0.75–0.78	-	H <sub>2</sub> O	[77]
<b>Arkachan, Russia</b>	200–385 (19)	3.7–26.3	0.84–1.07	1060–1830 (13)	CO <sub>2</sub> + H <sub>2</sub> O	[78]
Canan area, Honduras	240–338 (8)	0.9–6.2	0.68–0.83	-	H <sub>2</sub> O	[79]
<b>Zhaishang, China</b>	92–372 (20)	0.2–23.1	0.71–1.03	238–781 (20)	H <sub>2</sub> O	[80]
Qiangma, China	145–365 (18)	0.0–12.7	-	1750–2810 (4)	CO <sub>2</sub> + H <sub>2</sub> O	[81]
<b>Dongfeng, China</b>	117–341 (6)	0.5–11.7	0.57–1.00	2260–3380 (2)	CO <sub>2</sub> + H <sub>2</sub> O	[82]
<b>Linglong, China</b>	103–374 (8)	0.3–13.3	0.82–1.01	2280–3360 (2)	CO <sub>2</sub> + H <sub>2</sub> O	[82]
<b>Erdaogou, Xiaobeigou, China</b>	125–370 (46)	0.9–17.4	0.81–0.98	-	H <sub>2</sub> O	[83]
<b>Sanshandao, China</b>	101–390 (3)	0.2–18.4	0.75–0.78	-	H <sub>2</sub> O	[84]
Anjiayingzi, China	180–358 (11)	1.3–15.6	0.82–0.91	500–1100	CO <sub>2</sub> + H <sub>2</sub> O	[85]

Table 3. Cont.

Deposit, Region	Physicochemical Parameters of Fluids					Reference
	T, °C	Salinity *, wt.%	d, g/cm <sup>3</sup>	P, bar	Composition **	
Nancha, China	132–432 (12)	0.4–11.7	0.51–0.94	1520–3670 (3)	CO <sub>2</sub> + H <sub>2</sub> O	[86]
<b>Taishang, China</b>	158–336 (39)	0.2–9.1	0.73–0.92	-	H <sub>2</sub> O	[87]
Jinchangyu, China	120–410 (10)	3.0–28.3	-	-	CO <sub>2</sub> + H <sub>2</sub> O	[88]
Hetai, China	130–310 (4)	2.7–13.9	0.70–1.02	500–1710 (4)	CO <sub>2</sub> + H <sub>2</sub> O	[89]
Liyuan, China	136–408 (18)	0.5–12.6	0.65–0.98	1310–3470 (4)	CO <sub>2</sub> + H <sub>2</sub> O	[90]
Baolun, China	140–376 (6)	3.0–9.0	-	1000–1600 (2)	CO <sub>2</sub> + H <sub>2</sub> O	[91]
Gezhen, China	140–370 (8)	0.5–10.5	-	-	H <sub>2</sub> O	[91]
<b>Dongping, China</b>	154–382 (68)	0.1–35.4	-	1000 (1)	CO <sub>2</sub> + H <sub>2</sub> O	[92]
Xiadian, China	111–418 (16)	0.2–22.9	0.61–1.11	400–2470 (4)	CO <sub>2</sub> + H <sub>2</sub> O	[93]
<b>Luoshan, China</b>	212–393 (12)	3.0–9.1	0.47–0.92	770–1850 (2)	CO <sub>2</sub> + H <sub>2</sub> O	[94]
Fushan, China	211–380 (18)	0.0–11.2	0.43–0.98	770–1850 (2)	CO <sub>2</sub> + H <sub>2</sub> O	[94]
Bake, China	157–402 (12)	2.2–13.7	-	460–800 (5)	CO <sub>2</sub> + H <sub>2</sub> O	[95]
Chanziping, China	138–156 (18)	1.8–11.9	-	400–960 (12)	CO <sub>2</sub> + H <sub>2</sub> O	[95]
Dagaowu, China	176 (2)	4.9–9.6	-	460 (1)	CO <sub>2</sub> + H <sub>2</sub> O	[95]
Fenshuiao, China	178–183 (2)	10.1–10.2	-	220–680 (2)	CO <sub>2</sub> + H <sub>2</sub> O	[95]
Gaokeng, China	171 (2)	6.5–10.5	-	450 (1)	CO <sub>2</sub> + H <sub>2</sub> O	[95]
Hamashi, China	145–421 (3)	2.9–13.1	-	-	H <sub>2</sub> O	[95]
Huangjindong, China	225–397 (9)	3.6–10.9	-	990 (2)	CO <sub>2</sub> + H <sub>2</sub> O	[95]
Huangshan, China	156–350 (3)	1.2–24.0	-	420–590 (2)	CO <sub>2</sub> + H <sub>2</sub> O	[95]
Huangtudian, China	190–260 (2)	6.6–6.9	-	390–480 (2)	CO <sub>2</sub> + H <sub>2</sub> O	[95]
<b>Jinshan, China</b>	109–372 (53)	0.6–16.5	-	350–950 (10)	CO <sub>2</sub> + H <sub>2</sub> O	[95]
Kengtou, China	148–160 (2)	6.4–9.1	-	390 (1)	CO <sub>2</sub> + H <sub>2</sub> O	[95]
Miaoxiafan, China	158 (2)	4.1–9.2	-	410 (1)	CO <sub>2</sub> + H <sub>2</sub> O	[95]
Mobin, China	170–203 (9)	9.3–2.1	-	210–790 (4)	CO <sub>2</sub> + H <sub>2</sub> O	[95]
Pingshui, China	214–282 (6)	1.2–8.7	-	-	H <sub>2</sub> O	[95]
Taojinchong, China	107–352 (37)	0.5–20.1	-	580–770 (2)	CO <sub>2</sub> + H <sub>2</sub> O	[95]
Tonggu, China	97–300 (11)	1.1–10.4	-	-	H <sub>2</sub> O	[95]
Tongshulin, China	183 920	3.9–9.9	-	480 910	CO <sub>2</sub> + H <sub>2</sub> O	[95]
Wangu, China	138–310 (26)	0.8–12.6	-	-	H <sub>2</sub> O	[95]
Xi'an, China	147–325 (8)	3.3–8.5	-	660 (1)	CO <sub>2</sub> + H <sub>2</sub> O	[95]
Xichong, China	200–304 (5)	6.1–7.5	-	480 (2)	CO <sub>2</sub> + H <sub>2</sub> O	[95]
Xintang, China	125 (2)	2.9–4.2	-	320 (1)	CO <sub>2</sub> + H <sub>2</sub> O	[95]
Yanghanwu, China	151–185 (4)	3.4–8.2	-	400–480 (2)	CO <sub>2</sub> + H <sub>2</sub> O	[95]

Notes: \* salinity of fluid expressed in wt% NaCl equiv.; \*\* composition of gas phase of fluid inclusions; Number of determinations is shown in parentheses.

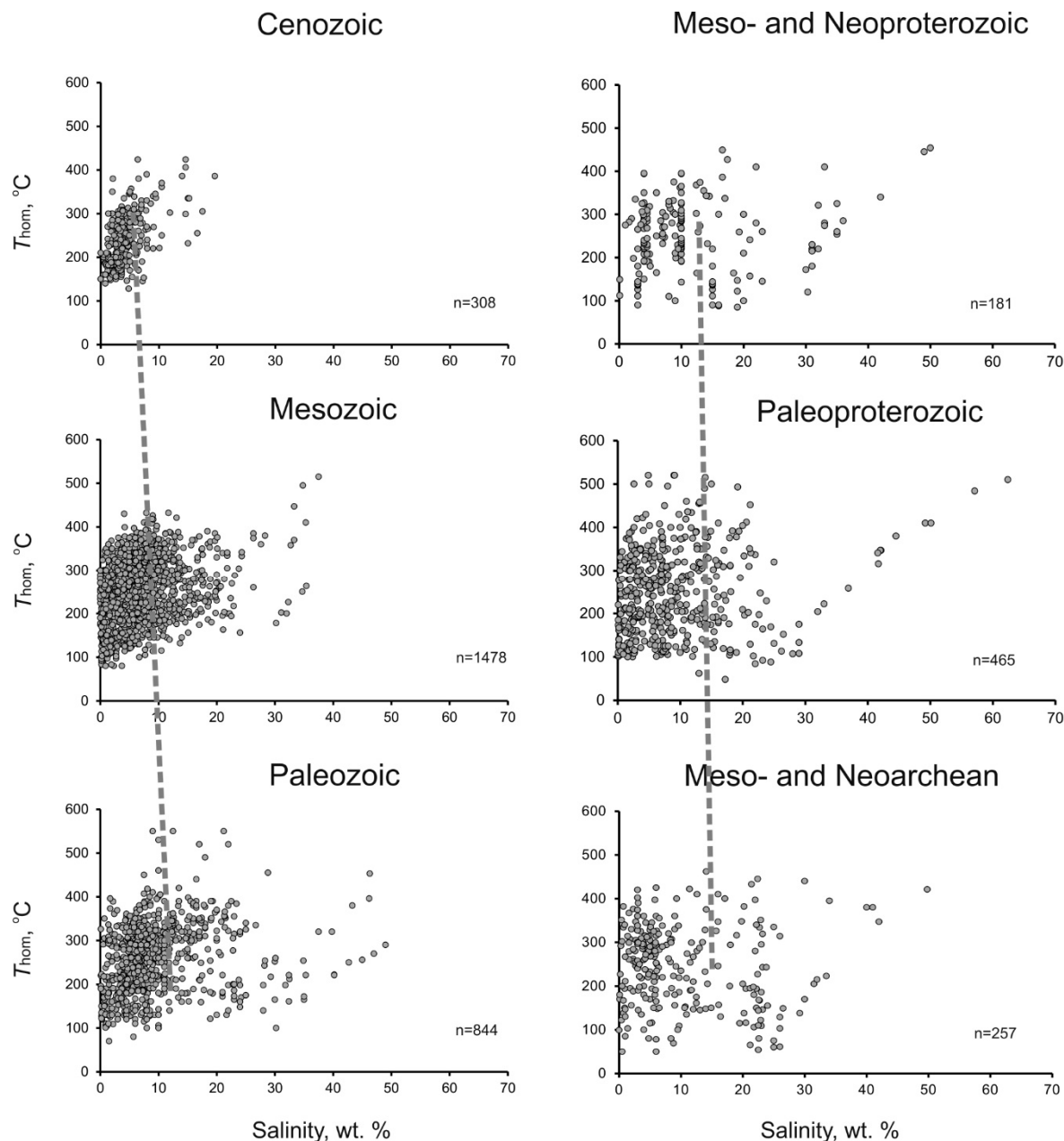


**Figure 1.** Temperature–salt concentration diagrams for mineralizing fluids at gold deposits of different age. Here and in Figures 2–5,  $n$  is the number of measurements. Here and on Figure 2 trendlines are shown as dashed lines. The initial data on the fluid parameters are provided as Supplementary Materials.

### 3.3. Paleozoic Deposits

Parameters of fluids that produced orogenic gold deposits are summarized in Table 4 and Figures 1–5 (844 temperature and fluid salinity estimates and 375 pressure estimates). Some of the deposits were formed in the one-phase fluid field above the appropriate solvi, including Hill End goldfield, Flying Pig, Tyrconnel, Charters Towers, Stawell-Magdala, Maldon, Mount Piper, Woods Point, and Walhalla, Australia; Haut Allier, Biards district, and Moulin de Cheni, France; Pataz region, Peru; Vorontsovskoye, Russia; and Jiapigou, Bulong, Qingshui, and Woxi, China. Most of them, however, formed from heterogeneous fluids, with H<sub>2</sub>O- and CO<sub>2</sub>-dominant fluid endmembers. The fluids forming the gold deposits had temperatures of 70 to 550 °C (median 267 °C), salinities of 0.1 to 49.0 wt.% NaCl equiv. (median 7.3 wt.% NaCl equiv.), and fluid pressure of 80–5030 bar (median 1500 bar) (Table 8). The comparison of homogeneous aqueous fluids with the aqueous phase

of the heterogeneous fluids revealed the slightly narrower range of homogenization temperatures (92–455 °C) and salinities (0.2–46.2 wt.% NaCl equiv) of the first ones.

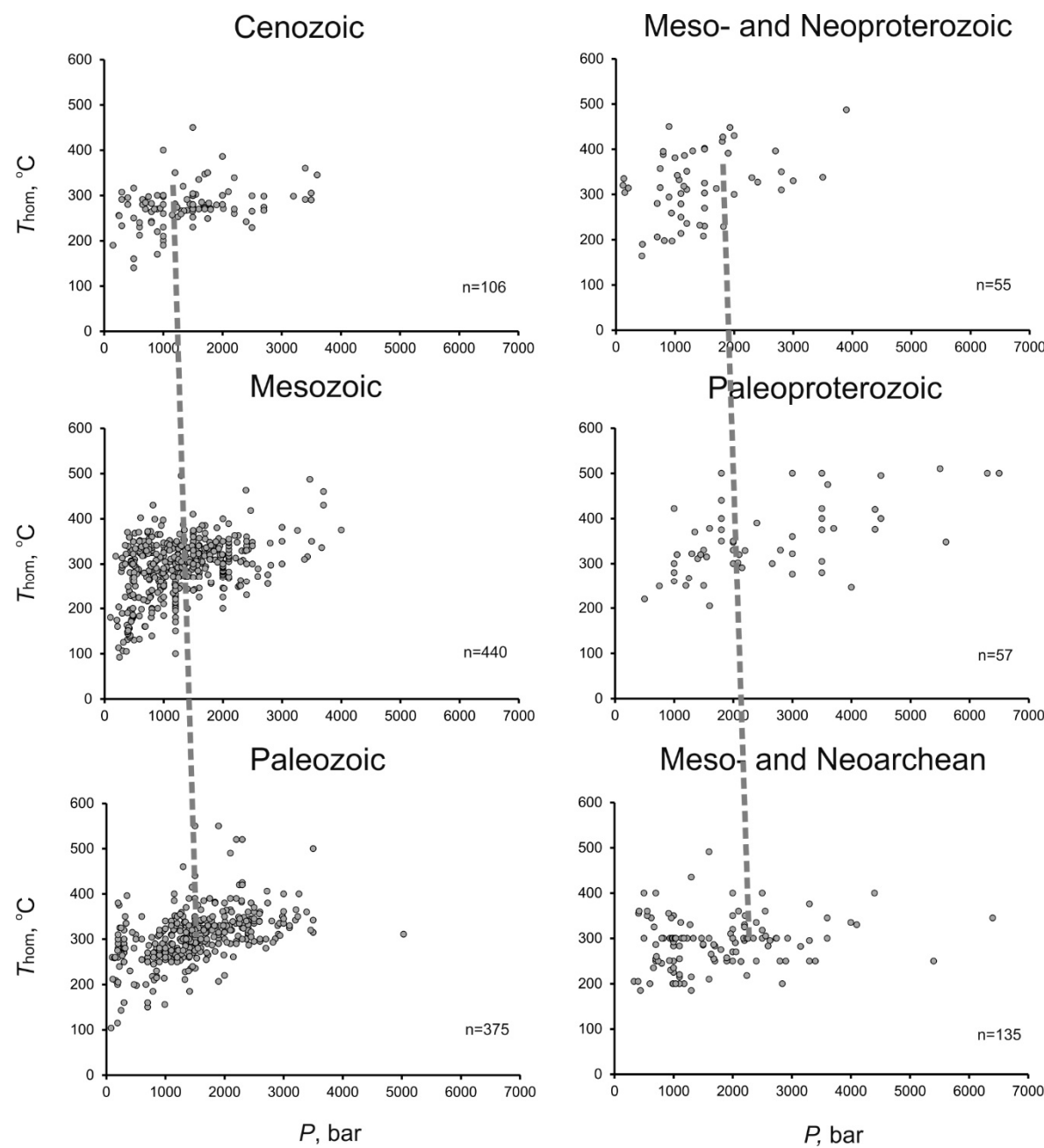


**Figure 2.** Temperature–pressure diagrams for mineralizing fluids at gold deposits of different age.

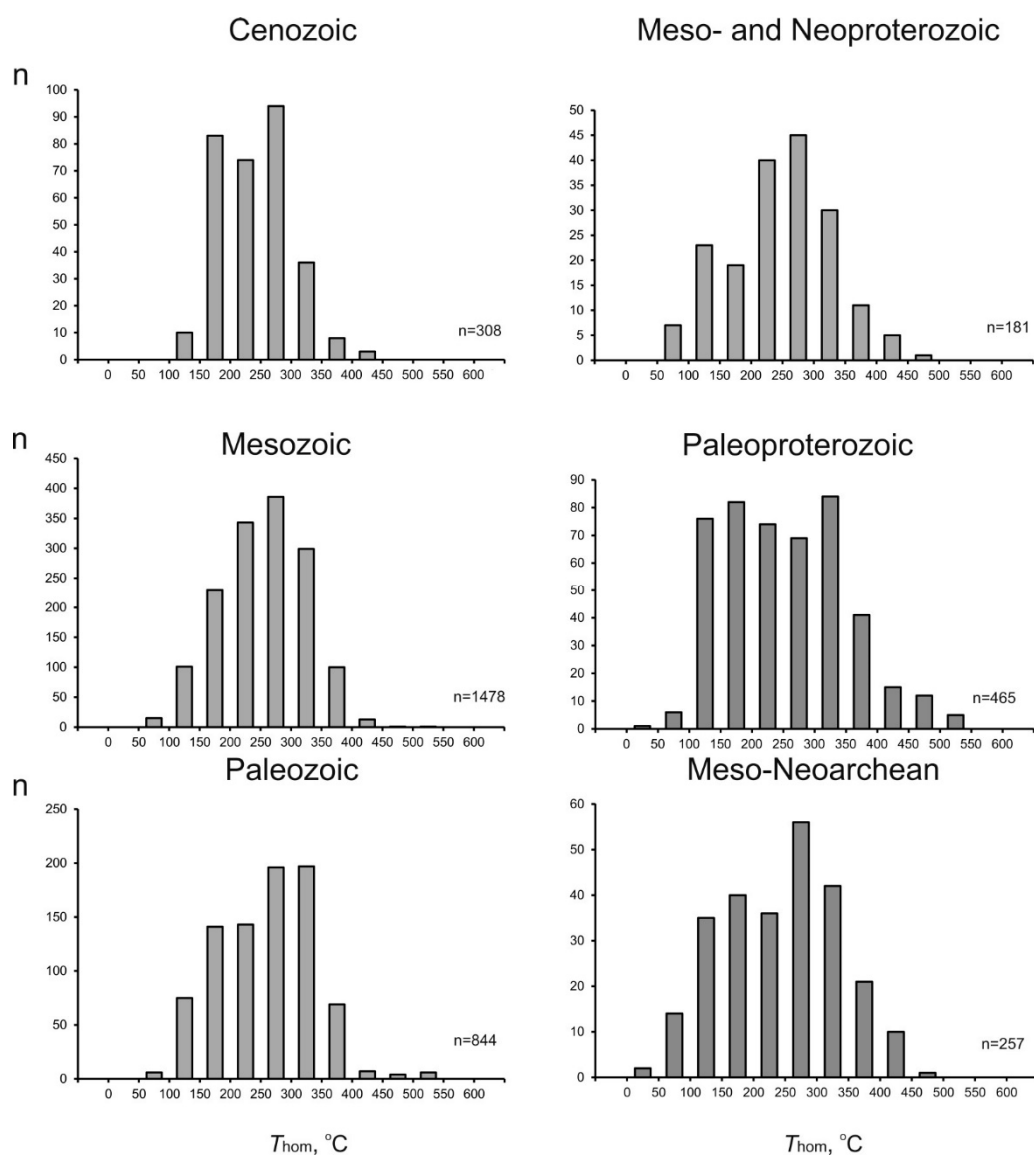
#### 3.4. Meso- and Neoproterozoic Deposits

Table 5 and Figures 1–5 show characteristics of the mineral-forming fluids of orogenic gold deposits. The information of the deposits comprises 181 temperature and fluid salinity estimates and 55 pressure estimates. A few of these deposits were formed in the one-phase fluid field above the appropriate solvi (e.g., Paiol mine, Brazil; and Udereyskoye, Russia). Most of the deposits were formed from fluids trapped in the two-phase field, with H<sub>2</sub>O- and CO<sub>2</sub>- or N<sub>2</sub>-dominant fluid endmembers. Ore-forming fluids for the gold deposits had ranges of temperature of 85–454 °C (median 255 °C), salinity of 0.1–50.0 wt.% NaCl equiv. (median 10.0 wt.% NaCl equiv.), and fluid pressure of 120–3900 bar (median 1200 bar) (Table 8). Again, as in the previous case, homogenization

temperatures (90–410 °C) and salinities (3.0–33.0 wt.% NaCl equiv) are varied in the narrower ranges than the parameters of the aqueous phase of the heterogeneous fluids (temperature of 85–454 °C, salinity 0.1–50.0 wt.% NaCl equiv).

### 3.5. Paleoproterozoic Deposits

Table 6 and Figures 1–5 show characteristics of the mineral-forming fluids of orogenic gold deposits. The information of the deposits comprises 465 temperature and fluid salinity estimates and 57 pressure estimates. These deposits typically contain fluid inclusions of two types: aqueous fluid of different salinity and homogeneous fluid of high-density gases. The gas inclusions are dominated by either CO<sub>2</sub> or N<sub>2</sub>. Inclusions of the two types not always occur in association with one another, and hence, pressure was evaluated not for all of the deposits. Ore-forming fluids for the gold deposits had ranges of temperature of 48–520 °C (median 252 °C), salinity of 0.5–62.4 wt.% NaCl equiv. (median 7.1 wt.% NaCl equiv.), and fluid pressure of 500–6500 bar (median 2080 bar) (Table 8).



**Figure 3.** Histograms of the temperatures of mineralizing fluids at gold deposits of different age.

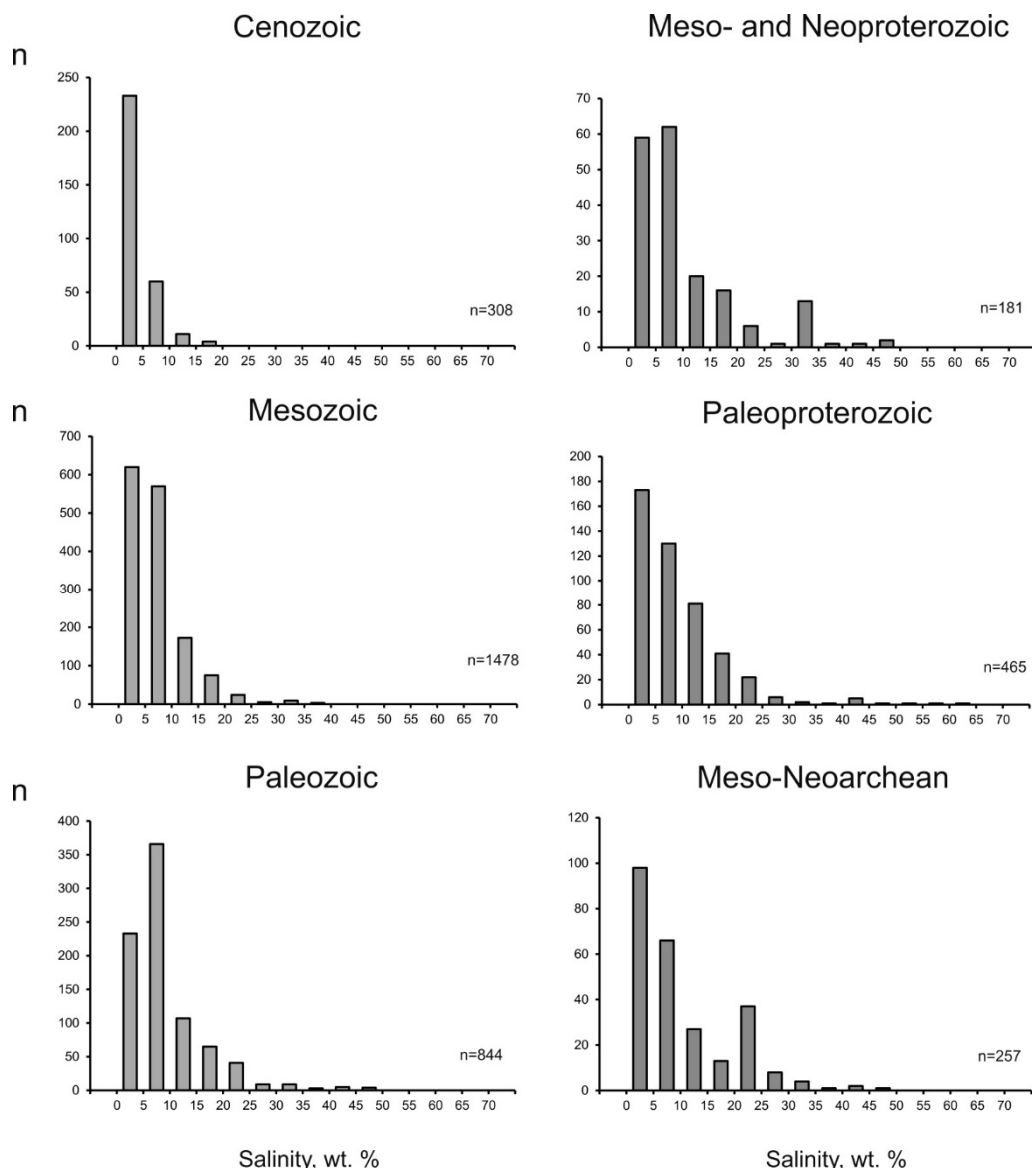


**Figure 4.** Histograms of the salinity of mineralizing fluids at gold deposits of different age.

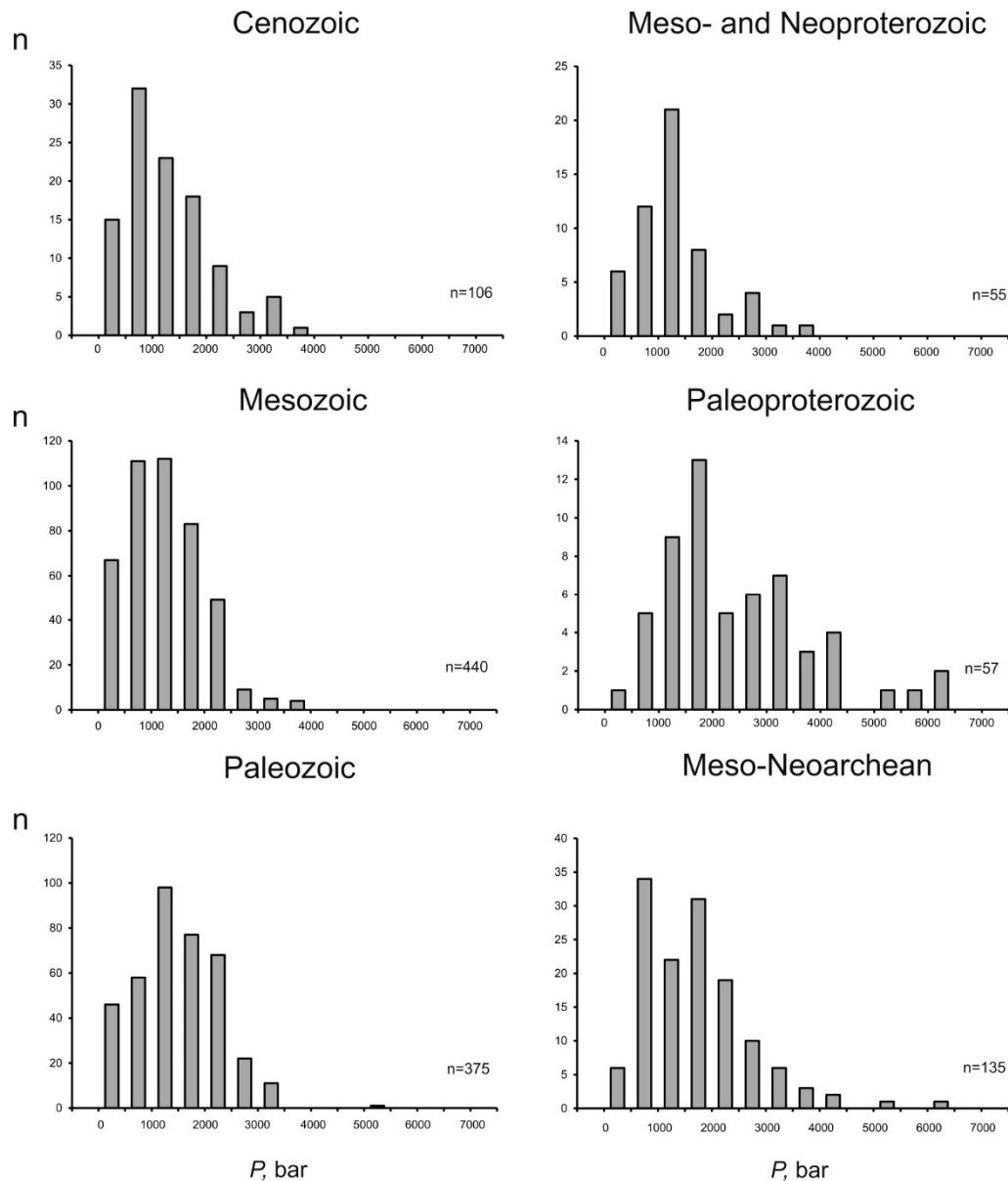


**Figure 5.** Histograms of the pressure of mineralizing fluids at gold deposits of different age.

### 3.6. Meso-Neoarchean Deposits

Parameters for the fluids from orogenic gold deposits are summarized in Table 7 and Figures 1–5. A few deposits were produced by trapping of a homogeneous aqueous or gaseous fluid (e.g., Kolar and Hutti, India, and Wiluna, Australia), but most deposits formed by trapping of heterogeneous fluids, with H<sub>2</sub>O- and CO<sub>2</sub>- or CH<sub>4</sub>-dominant fluid endmembers. The ore-forming fluids had a temperature range of 50–462 °C (median 254 °C), salinity of 0.0–49.8 wt.% NaCl equiv. (median 6.1 wt.% NaCl equiv.), and fluid pressure of 330 to 6400 bar (median 1680 bar) (Table 8).

It should be noted that, for all time intervals under consideration, the parameters of fluids from which the large gold deposits (>100 tonnes Au) were formed do not differ from the total sample of corresponding time (Table 9).

**Table 4.** Parameters of mineralizing fluids of Paleozoic gold deposits.

Deposit, Region	Physicochemical Parameters of Fluids					Reference
	T, °C	Salinity *, wt. %	d, g/cm³	P, bar	Composition **	
Hill End goldfield, Australia	260–360 (2)	2.4	0.59–0.80	-	H <sub>2</sub> O	[96]
Haut Allier, France	260–420 (10)	0.5–8.1	0.44–0.85	-	H <sub>2</sub> O	[97]
Kvartsytovye gorki, Kazakhstan	255–305 (7)	6.0–7.0	0.93–0.94	275–900 (4)	CO <sub>2</sub> + CH <sub>4</sub> + H <sub>2</sub> O	[98]
<b>Zholymbet, Kazakhstan</b>	255–345 (45)	7.0–17.0	0.89–1.04	1000–2100 (4)	CO <sub>2</sub> + H <sub>2</sub> O	[98]
<b>Bestobe, Kazakhstan</b>	270–315 (19)	5.0–14.0	1.03–1.08	900–1600 (8)	CO <sub>2</sub> + CH <sub>4</sub> + H <sub>2</sub> O	[98]
N. Aksu, Kazakhstan	305–365 (20)	12.0–17.0	0.94–1.01	1400–2600 (8)	CO <sub>2</sub> + CH <sub>4</sub> + H <sub>2</sub> O	[98]
Stepnyak, Kazakhstan	270–365 (14)	11–13.0	0.96–1.03	1100–1800 (6)	CO <sub>2</sub> + H <sub>2</sub> O	[98]
<b>S. Aksu, Kazakhstan</b>	190–345 (44)	8.0–12.0	0.89–1.05	1200–2800 (8)	CO <sub>2</sub> + CH <sub>4</sub> + H <sub>2</sub> O	[98]
Zhana-Tyube, Kazakhstan	255–355 (43)	9.0–12.0	0.88–1.08	1250–3500 (11)	CO <sub>2</sub> + CH <sub>4</sub> + H <sub>2</sub> S + H <sub>2</sub> O	[98]
Flying Pig, Australia	135–370 (32)	1.1–10.1	0.56–0.96	-	H <sub>2</sub> O	[99]
Tyrconnel, Australia	280 (1)	4.7	0.8	-	H <sub>2</sub> O	[99]
Pataz region, Peru	130–320 (9)	7.0–37.5	0.76–1.06	-	H <sub>2</sub> O	[100]
Saralinskoye, Russia	150–365 (8)	6.3–29.3	0.77–1.07	770–2900 (12)	CO <sub>2</sub> + CH <sub>4</sub> + H <sub>2</sub> O	[101]
Nagambie, Australia	130–305 (7)	3.7–6.4	0.76–0.96	850–1100 (2)	CO <sub>2</sub> + H <sub>2</sub> O	[102]
Kommunar, Russia	210–340 (50)	7.9–15.2	0.89–1.06	930–3500 (11)	CO <sub>2</sub> + CH <sub>4</sub> , H <sub>2</sub> O	[103]
<b>Zarmitan, Uzbekistan</b>	270–380 (16)	3.5–20.0	0.74–1.07	820–2730 (30)	CO <sub>2</sub> + CH <sub>4</sub> + H <sub>2</sub> O	[104]
Deborah, Australia	220–400 (3)	0.1–10.0	0.65–0.93	2000–3000 (2)	CO <sub>2</sub> + CH <sub>4</sub> + H <sub>2</sub> O	[105]
<b>Sukhoi log, Russia</b>	165–380 (45)	3.7–9.5	0.72–1.06	230–2450 (28)	CO <sub>2</sub> + CH <sub>4</sub> + N <sub>2</sub> + H <sub>2</sub> O	[106]
<b>Berezovskoye, Russia</b>	270–365 (14)	9.5–26.7	0.91–1.09	1470–3460 (21)	CO <sub>2</sub> + H <sub>2</sub> O	[107]
Fosterville, Australia	170 (1)	0.5	0.90	-	H <sub>2</sub> O	[108]
Vorontsovskoye, Russia	100–150 (7)	6.4–9.2	0.98–1.00	-	H <sub>2</sub> O	[39]
Biards district, France	125–375 (6)	1.7–7.4	0.54–0.97	-	H <sub>2</sub> O	[109]
Mayskoye, Russia	100–455 (29)	1.4–42.7	0.63–1.28	-	CO <sub>2</sub> + CH <sub>4</sub> + H <sub>2</sub> O	[110]
CSA deposit, Cobar, Australia	200–350 (4)	0.1–5.0	0.66–0.91	1500–2000 (4)	CO <sub>2</sub> + H <sub>2</sub> O	[111]
Moulin de Cheni, France	150–250 (2)	4.0–8.0	0.87–0.95	-	H <sub>2</sub> O	[112]
Jiapigou, China	150–350 (4)	0.7–6.5	0.58–0.93	-	H <sub>2</sub> O	[113]
Bulong, China	160–395 (30)	5.3–46.2	0.63–1.18	-	H <sub>2</sub> O	[114]
<b>Charters Tauers, Australia</b>	80–305 (19)	0.2–28.3	0.71–1.08	-	H <sub>2</sub> O	[115]
Sarekoubu, China	255–395 (5)	-	-	-	CO <sub>2</sub> + CH <sub>4</sub> + H <sub>2</sub> O, H <sub>2</sub> O	[116]
Qingshui, China	155–355 (3)	3.1–7.5	0.69–0.94	-	H <sub>2</sub> O	[117]
Tanjiashan, China	120–320 (5)	3.7–10.8	0.80–1.00	-	CO <sub>2</sub> + CH <sub>4</sub> + H <sub>2</sub> O	[118]
Sandwich Point, Canada	150–335 (26)	2.0–25.0	0.69–1.09	-	CO <sub>2</sub> + CH <sub>4</sub> + H <sub>2</sub> O	[119]
Fosterville, Australia	119–264	0.1–10.7	0.88–0.95	1800–2400	CO <sub>2</sub> + CH <sub>4</sub> + N <sub>2</sub> + H <sub>2</sub> O	[120]
<b>Stawell-Magdalas, Australia</b>	110–238	1.4–5.6	0.86–0.97	-	H <sub>2</sub> O	[120]
<b>Bendigo, Australia</b>	84–315	0.9–7.8	0.77–0.94	1400–1600	CO <sub>2</sub> + CH <sub>4</sub> + N <sub>2</sub> + H <sub>2</sub> O	[120]
Wattle Gully, Australia	70–225	1.5–6.3	-	1600	CO <sub>2</sub> + CH <sub>4</sub> + N <sub>2</sub> + H <sub>2</sub> O	[120]
Maldon (1), Australia	177–187	20.3–21.6	0.85–1.04	-	H <sub>2</sub> O	[120]
Maldon (2), Australia	101–379	0.9–13.4	0.74–0.97	-	H <sub>2</sub> O	[120]
Mount Piper, Australia	92–331	0.7–7.1	0.74–0.90	-	H <sub>2</sub> O	[120]
Woods Point, Australia	129–279	1.6–4.0	0.78–0.95	-	H <sub>2</sub> O	[120]
Walhalla, Australia	122–283	0.2–6.9	0.85–0.94	-	H <sub>2</sub> O	[120]
Bogunayskoye, Russia	110–350 (88)	0.2–49.0	0.73–1.22	100–1600 (31)	CO <sub>2</sub> + CH <sub>4</sub> + N <sub>2</sub> + H <sub>2</sub> S, H <sub>2</sub> O	[121]
Annage, China	140–380 (42)	0.5–22.0	0.71–1.02	790–1300 (2)	CO <sub>2</sub> + CH <sub>4</sub> + H <sub>2</sub> O	[122]
Woxi, China	178–357 (24)	1.6–9.3	0.71–0.88	-	H <sub>2</sub> O	[123]
Huangshan, China	127–376 (34)	0.2–9.6	0.65–0.94	870–2610 (34)	CO <sub>2</sub> + H <sub>2</sub> O	[124]
Yingchengzi, China	104–400 (12)	1.1–12.4	0.62–0.97	80–3260 (9)	CO <sub>2</sub> + H <sub>2</sub> O	[125]
Limarinho, Portugal	180–330 (6)	3.0–7.3	0.73–0.91	600–3500 (6)	CO <sub>2</sub> + CH <sub>4</sub> + N <sub>2</sub> + H <sub>2</sub> O	[126]
<b>Vasil'kovskoe, Kazakhstan</b>	120–550(90)	2.0–20.0	0.46–0.96	200–2500 (68)	CO <sub>2</sub> + CH <sub>4</sub> + N <sub>2</sub> + H <sub>2</sub> O	[127]
Woxi, China	109–396 (35)	0.1–12.5	-	140–470 (10)	CO <sub>2</sub> + H <sub>2</sub> O	[95]
<b>Sukoi Log, Russia</b>	130–385 (61)	3.7–9.5	0.65–1.09	640–2630 (35)	CO <sub>2</sub> + CH <sub>4</sub> + N <sub>2</sub> + H <sub>2</sub> O	[128]
<b>Verninskoye, Russia</b>	136–356 (31)	1.4–8.1	0.84–1.05	570–3150 (10)	CO <sub>2</sub> + H <sub>2</sub> O	[128]
Dogaldyn, Russia	128–339 (12)	1.4–7.3	0.90–1.05	960–3230 (10)	CO <sub>2</sub> + H <sub>2</sub> O	[128]
Uryakh, Russia	191–361 (7)	2.5–9.1	0.94–1.08	1050–3290 (6)	CO <sub>2</sub> + H <sub>2</sub> O	[128]
Irokinda, Russia	179–453 (31)	3.9–46.3	0.97–1.15	840–5030 (8)	CO <sub>2</sub> + H <sub>2</sub> O	[128]

Notes: \* salinity of fluid expressed in wt% NaCl equiv.; \*\* composition of gas phase of fluid inclusions; Number of determinations is shown in parentheses.

**Table 5.** Parameters of ore-forming fluids of Meso- and Neoproterozoic gold deposits.

Deposit, Region	Physicochemical Parameters of Fluids					Reference
	T, °C	Salinity *, wt.%	d, g/cm³	P, bar	Composition **	
Olimpiadinskoye, Russia	105–410 (2)	1.9–28.7	0.68–0.93	255–3045 (29)	CO <sub>2</sub> + CH <sub>4</sub> + N <sub>2</sub> + H <sub>2</sub> S, H <sub>2</sub> O	[129]
Cachoeira de Minas, Sao Francisco, Brazil	250–350 (2)	6.0	0.68–0.86	2000 (1)	CO <sub>2</sub>	[130]
Veduga, Russia	164–368 (12)	8.2–19.3	0.72–1.04	120–1820 (8)	CO <sub>2</sub> + CH <sub>4</sub> , CH <sub>4</sub> , H <sub>2</sub> O	[131]
Olimpiadinskoye, Russia	190–449 (10)	4.8–17.4	0.67–0.92	450–2700 (11)	CH <sub>4</sub> , N <sub>2</sub> , CO <sub>2</sub> + N <sub>2</sub> , H <sub>2</sub> O	[131]
Harnas area, Sweden	85–395 (84)	3.0–19.0	0.48–1.11	-	CO <sub>2</sub> , H <sub>2</sub> O	[132]
Paiol mine, Brazil	90–410 (16)	3.0–33.0	0.81–1.07	-	H <sub>2</sub> O	[133]
Udereyskoye, Russia	120–180 (2)	30.3	1.12–1.20	-	H <sub>2</sub> O	[56]
Tunkillia, Nuckulla Hill, Barns, and Weenannna, Central Gawler Craton, Australia	88–350 (18)	0.1–23.0	0.68–1.13	-	CO <sub>2</sub> , H <sub>2</sub> O	[134]
Tarcoola gold field, S. Australia	265–335 (9)	1.6–6.7	0.69–0.92	-	CO <sub>2</sub> + CH <sub>4</sub> , H <sub>2</sub> O	[135]
Telfer, Australia	143–454 (135)	2.0–50.0	-	1500–3000 (2)	CO <sub>2</sub> , H <sub>2</sub> O	[136]

Notes: \* salinity of fluid expressed in wt% NaCl equiv.; \*\* composition of gas phase of fluid inclusions; Number of determinations is shown in parentheses.

**Table 6.** Parameters of ore-forming fluids of Paleoproterozoic gold deposits.

Deposit, Region	Physicochemical Parameters of Fluids					Reference
	T, °C	Salinity *, wt.%	d, g/cm³	P, bar	Composition **	
Tartan Lake, Canada	250–390 (4)	2.2–12.6	0.44–0.91	1200–2400 (2)	CO <sub>2</sub> , H <sub>2</sub> O	[137]
Star Lake, Canada	100–520 (112)	0.5–42.1	0.30–1.40	1000–6300 (14)	CO <sub>2</sub> + CH <sub>4</sub> , H <sub>2</sub> O	[138]
Flin Flon Domain, Canada	174–331 (20)	0.4–16.2	0.65–1.01	-	CO <sub>2</sub> , H <sub>2</sub> O	[139]
Pirila, Finland	130–325 (4)	1.8–25.0	0.87–1.00	1500–1800 (2)	CO <sub>2</sub> + CH <sub>4</sub> , H <sub>2</sub> O	[140]
Star Lake (La Ronge), Canada	160–340 (5)	1.3–8.2	0.69–0.97	-	CO <sub>2</sub> , H <sub>2</sub> O	[141]
Caxias, Brazil	205–378 (2)	10.8	0.70–0.95	1600–3700 (3)	CO <sub>2</sub> + N <sub>2</sub> , H <sub>2</sub> O	[142]
Fazenda Canto, Brazil	280–500 (6)	2.6–4.0	0.72–0.93	1000–3500 (4)	CO <sub>2</sub> + CH <sub>4</sub> + N <sub>2</sub> , H <sub>2</sub> O	[143]
Fazenda Maria Preta, Brazil	320–420 (2)	-	-	2100–4400 (2)	CO <sub>2</sub> + CH <sub>4</sub> + N <sub>2</sub> , H <sub>2</sub> O	[143]
Fazenda Brasileiro, Brazil	400–500 (7)	-	-	1800–6500 (7)	CO <sub>2</sub> + CH <sub>4</sub> + N <sub>2</sub> , H <sub>2</sub> O	[143]
Guarim, Brazil	140–310 (4)	5.6–5.7	0.76–0.97	860–2900 (4)	CO <sub>2</sub> + CH <sub>4</sub> + N <sub>2</sub> , H <sub>2</sub> O	[144]
Batman, Australia	242–458 (17)	1.8–20.6	0.45–0.96	-	CO <sub>2</sub> + CH <sub>4</sub> , CH <sub>4</sub> , H <sub>2</sub> O	[145]
Serrinha, Brazil	280–430 (4)	4.5–21.0	0.44–0.93	1300–3000 (2)	CO <sub>2</sub> + CH <sub>4</sub> + N <sub>2</sub> , H <sub>2</sub> O	[146]
Callie, Australia	48–404 (61)	0.5–33.0	0.52–1.19	-	CO <sub>2</sub> + CH <sub>4</sub> + N <sub>2</sub> , H <sub>2</sub> O	[147]
Coyote Prospect, Australia	183–434 (10)	0.1–12.5	0.55–0.98	-	CO <sub>2</sub> + CH <sub>4</sub> + N <sub>2</sub> , H <sub>2</sub> O	[147]
Groudrust, Australia	161–490 (9)	0.2–13.9	0.49–0.97	-	CO <sub>2</sub> + CH <sub>4</sub> + N <sub>2</sub> , H <sub>2</sub> O	[147]
Tanami gold field, Australia	101–452 (48)	0.1–21.2	0.57–1.10	-	CO <sub>2</sub> + CH <sub>4</sub> + N <sub>2</sub> , H <sub>2</sub> O	[147]
Angovia, W. Africa	156–370 (20)	1.2–8.4	0.69–0.98	1050–1350 (2)	CO <sub>2</sub> + CH <sub>4</sub> + N <sub>2</sub>	[148]
Chega Tudo, Brazil	100–371 (42)	0.2–12.3	0.52–1.04	2000–3000 (2)	CO <sub>2</sub> + CH <sub>4</sub> , CO <sub>2</sub> , H <sub>2</sub> O	[149]
Bjorkdal, Sweden	136–400 (13)	2.2–14.0	0.55–1.01	500–1800 (2)	CO <sub>2</sub> , H <sub>2</sub> O	[150]
Carara, Brazil	264–346 (2)	5.0–5.4	0.66–0.82	1800–3600 (2)	CO <sub>2</sub> + CH <sub>4</sub> + N <sub>2</sub>	[151]
<b>Morila, W. Africa</b>	175–339 (8)	3.0–20.3	0.65–1.03	-	CH <sub>4</sub> + N <sub>2</sub> , H <sub>2</sub> O	[152]
Baboto, Mali, W Africa	255–320 (3)	1.5–10.7	0.80–0.81	-	CO <sub>2</sub> + CH <sub>4</sub> + N <sub>2</sub> + H <sub>2</sub> O	[153]
Gara, Mali, W. Africa	140–380 (15)	4.5–57.1	0.78–1.24	750–2200 (4)	CO <sub>2</sub> + CH <sub>4</sub> + N <sub>2</sub> + H <sub>2</sub> O	[153]
Loulou-3, Mali, W Africa	170–310 (12)	0.2–11.7	0.75–0.93	1550 (1)	CO <sub>2</sub> + CH <sub>4</sub> + N <sub>2</sub> + H <sub>2</sub> O	[153]
<b>Yalea, Mali, W. Africa</b>	175–519 (15)	0.7–62.4	0.75–1.60	1450 (1)	CO <sub>2</sub> + CH <sub>4</sub> + N <sub>2</sub> + H <sub>2</sub> O	[153]
<b>Piaba, Brasil</b>	183–377	2.5–7.2	0.96–0.99	1250–2080	CO <sub>2</sub> + CH <sub>4</sub> , H <sub>2</sub> O	[154]
Turmalina, Brazil	106–393 (18)	0.2–23.8	-	1000–2000	CO <sub>2</sub> , H <sub>2</sub> O	[155]
<b>Piaba, Brasil</b>	180–360	2.5–7.2	-	1500–2800	CO <sub>2</sub> , H <sub>2</sub> O	[156]
Julie, Ghana	210–275 (28)	1.9–8.6	0.41–0.99	-	CO <sub>2</sub> , H <sub>2</sub> O	[157]
Lamego, Brazil	300–375 (18)	2.0–9.0	0.68–0.94	2660–3500 (3)	CO <sub>2</sub> + CH <sub>4</sub>	[158]

Notes: \* salinity of fluid expressed in wt% NaCl equiv.; \*\* composition of gas phase of fluid inclusions; Number of determinations is shown in parentheses.

**Table 7.** Parameters of mineralizing fluids of Meso-Neoarchean gold deposits.

Deposit, Region	Physicochemical parameters of fluids					Reference
	T, °C	Salinity *, wt.%	d, g/cm³	P, bar	Composition **	
Henderson, Canada	205–215 (2)	31.5–32.0	1.11–1.25	330–1300 (12)	CO <sub>2</sub> + H <sub>2</sub> O	[159]
<b>McInture-Hollinger, Canada</b>	175–348 (5)	6.1–19.8	0.79–1.00	-	CO <sub>2</sub> + CH <sub>4</sub> + N <sub>2</sub> + H <sub>2</sub> O	[160]
<b>Kolar, India</b>	210–420 (14)	3.0–12.0	0.70–0.85	1300–1600 (2)	CO <sub>2</sub>	[161]
Renabie, Canada	161–360 (3)	6.0–12.5	0.89–1.00	2550 (1)	CO <sub>2</sub> + H <sub>2</sub> O	[162]
Mink Lake, Canada	250–345 (7)	5.3–6.1	0.65–0.85	-	CO <sub>2</sub> + H <sub>2</sub> O	[163]
<b>Sigma, Canada</b>	60–395 (17)	25.0–34.0	0.65–1.07	2000 (1)	CO <sub>2</sub> + CH <sub>4</sub> , H <sub>2</sub> O	[164]
<b>Kolar, India</b>	235–340 (75)	-	0.57–1.24	700–6400 (24)	CO <sub>2</sub> + CH <sub>4</sub>	[165]
<b>Pamour, Canada</b>	260–325 (7)	3.5–6.0	0.70–0.81	-	CO <sub>2</sub> + CH <sub>4</sub>	[166]
Abbots, South Africa	242–319 (2)	6.4	0.74–0.87	-	CO <sub>2</sub> + CH <sub>4</sub> + N <sub>2</sub> , H <sub>2</sub> O	[167]
Bellevue, South Africa	233–314 (2)	4.8	0.75–0.87	-	CO <sub>2</sub> + CH <sub>4</sub> + N <sub>2</sub> , H <sub>2</sub> O	[167]
Pioneer, South Africa	195–307 (4)	1.8–8.5	0.73–0.93	-	CO <sub>2</sub> + CH <sub>4</sub> + N <sub>2</sub> , H <sub>2</sub> O	[167]
<b>Surluga, Canada</b>	180–300 (30)	1.0–23.0	0.90–1.01	-	CO <sub>2</sub> + CH <sub>4</sub> + N <sub>2</sub> , H <sub>2</sub> O	[168]
<b>Sigma, Canada</b>	113–425 (8)	1–40	-	-	CO <sub>2</sub> + CH <sub>4</sub> + N <sub>2</sub> , H <sub>2</sub> O	[169]
Donalda, Canada	100–380 (6)	4–41	-	-	CO <sub>2</sub> + CH <sub>4</sub> + N <sub>2</sub> , H <sub>2</sub> O	[169]
Dumont-Bras d'Or, Canada	175–398 (6)	-	-	-	CO <sub>2</sub> + CH <sub>4</sub> + N <sub>2</sub>	[169]
<b>Champion Iode, Kolar, India</b>	138–421 (2)	29.2–49.8	1.08–1.14	3150–3600 (2)	CO <sub>2</sub> , H <sub>2</sub> O	[170]
Nundydroog mine, Kolar, India	170–440 (4)	5.0–30.0	0.86–1.13	-	CO <sub>2</sub> , H <sub>2</sub> O	[170]
<b>Wiluna, W. Australia</b>	243 (1)	23.2	1.02	-	H <sub>2</sub> O	[171]
Bronzewing, W. Australia	103–445 (47)	0.2–26.0	0.76–1.14	-	CO <sub>2</sub> + CH <sub>4</sub> , CH <sub>4</sub> , H <sub>2</sub> O	[172]
Siscoe, Canada	156–330 (6)	2.0–9.0	0.67–0.98	-	CO <sub>2</sub> + H <sub>2</sub> O	[173]
<b>Junction, W. Australia</b>	69–400 (7)	8.8–42.0	0.63–1.07	700–4400 (2)	CO <sub>2</sub> + CH <sub>4</sub> , H <sub>2</sub> O	[174]
Golden Eagle, Mosquito Creek belt, W. Australia	99–374 (10)	0.0–21.7	0.52–0.77	-	CO <sub>2</sub> + CH <sub>4</sub> , H <sub>2</sub> O	[175]
Orenada 2, Canada	65–195 (8)	4.8–26.5	1.00–1.14	-	CO <sub>2</sub> + CH <sub>4</sub> , H <sub>2</sub> O	[176]
<b>Hutti, India</b>	300 (2)	3.9–13.5	0.76–0.87	1000–1700 (2)	CO <sub>2</sub>	[177]
Golden Crown, W. Australia	257–376 (2)	2.3	0.48–0.82	500–3300 (6)	CO <sub>2</sub> + H <sub>2</sub> O	[178]
<b>Wiluna, W. Australia</b>	146–319 (3)	23.2–23.8	0.93–1.10	700–1680 (4)	CO <sub>2</sub> , H <sub>2</sub> O	[179]
Ramepuro, E. Finland	235–355 (3)	6.5–10.0	0.67–0.91	1000 (1)	CO <sub>2</sub> + CH <sub>4</sub> , CH <sub>4</sub>	[180]
<b>Woodcutters field, W. Australia</b>	210–462 (4)	5.7–14.1	0.76–0.90	-	CO <sub>2</sub> , H <sub>2</sub> O	[181]
McPhees, W. Australia	106–410 (9)	1.0–21.8	0.67–1.11	-	CO <sub>2</sub> + CH <sub>4</sub> + N <sub>2</sub> , H <sub>2</sub> O	[182]
<b>Tarmoola, W. Australia</b>	261–335 (8)	1.6–5.1	0.72–0.93	-	CO <sub>2</sub> , H <sub>2</sub> O	[183]
<b>Mount Charlotte, Australia</b>	220–312 (5)	4.5–5.7	0.74–0.89	1500–2200 (6)	CO <sub>2</sub> + CH <sub>4</sub> , H <sub>2</sub> O	[184]
<b>Giant, Canada</b>	180–360 (4)	4.0–9.0	0.60–0.96	1000–2000 (2)	CO <sub>2</sub> + CH <sub>4</sub> , H <sub>2</sub> O	[185]
<b>Uti, India</b>	180–397 (8)	0.5–22.0	0.55–1.01	930–2560 (4)	CO <sub>2</sub> + H <sub>2</sub> O	[186]
Primrose, Kwekwe, Zimbabwe	222–280 (6)	1.6–9.2	0.88–0.90	825–2780 (4)	CO <sub>2</sub> , H <sub>2</sub> O	[187]
Jojo, Kwekwe, Zimbabwe	145–219 (5)	-	0.97–0.99	990–3100 (4)	CO <sub>2</sub> , H <sub>2</sub> O	[187]
Indarama, Kwekwe, Zimbabwe	80–144 (3)	6.0–>22	1.02–1.23	1180–2850 (4)	CH <sub>4</sub> + N <sub>2</sub> , H <sub>2</sub> O	[187]
<b>Hutti, India</b>	205–280	1.7–6.4	-	500–2000	CO <sub>2</sub> + CH <sub>4</sub> , H <sub>2</sub> O	[188]
<b>Hira-Buddini, India</b>	128–320	0.5–22	0.67–1.09	-	CO <sub>2</sub> + CH <sub>4</sub> , H <sub>2</sub> O	[188]
Sunrise Dam, W. Australia	198–433 (18)	3.0–21.4	0.67–0.90	800–2930 (19)	CO <sub>2</sub> + H <sub>2</sub> O	[189]
Missouri, W. Australia	61–402 (16)	3.0–26.0	0.90–1.01	420–2630 (30)	CO <sub>2</sub> + CH <sub>4</sub> + H <sub>2</sub> S, CH <sub>4</sub>	[190]
Klipwal Gold Mine, South Africa	115–367 (316)	0.3–19.5	0.35–1.05	1100–2500 (4)	CO <sub>2</sub> + CH <sub>4</sub> , H <sub>2</sub> O	[191]

Notes: \* salinity of fluid expressed in wt% NaCl equiv.; \*\* composition of gas phase of fluid inclusions; Number of determinations is shown in parentheses.

#### 4. Discussion

Tables 8 and 9 summarize data on fluid parameters of orogenic deposits of different age. The compiled dataset was analyzed using binary temperature–salinity and pressure–temperature diagrams,

histograms, and boxplot diagrams. In addition, the Student's t-test was calculated in pairs for salinity and fluid pressure values to compare the average values of independent data samples, since the distribution of fluid parameters did not differ much from the normal distribution. The principal conclusions derived from this analysis are discussed below.

The binary plots indicate that the data of all of the discussed deposit-age-groups plot within a single field, with the ranges of the parameters shrinking from older to younger deposits mostly because of progressively narrower ranges of fluid pressure and salinity (Figures 1 and 2). Some fluid parameters (salinity and pressure) systematically and notably vary depending on the age of the mineralization. At the same time, the homogeneous character of the fields and a single field for all data points of a given set indicate that the data are homogeneous (pertain to a single fluid system). This led us to suggest that most of the analyzed fluid systems belong to a single type: one that produces orogenic gold mineralization.

**Table 8.** Median values of main physicochemical parameters of mineral-forming fluids of orogenic gold deposits.

Age, Ma	Temperature, °C	Salinity, wt.% NaCl Equiv	n	Pressure, bar	n
Cenozoic	242	3.6	308	1305	106
0–65	(128–424)	(0.0–19.6)		(150–3600)	
Mesozoic	260	5.9	1478	1200	440
65–252	(80–515)	(0.0–37.5)		(100–4000)	
Paleozoic	267	7.3	844	1500	375
2252–540	(70–550)	(0.1–49.0)		(80–5030)	
Meso- and Neoproterozoic	255	10.0	181	1200	55
540–1600	85–454	(0.1–50.0)		(120–3900)	
Paleoproterozoic	252	7.1	465	2080	57
1600–2500	(48–520)	(0.5–62.4)		(500–6500)	
Meso-Neoarchean	254	6.1	257	1680	135
2500–3200	(50–462)	(0.0–49.8)		(330–6400)	

n: Number of determinations; Minimum and maximum values are shown in parentheses.

**Table 9.** Median values of main physicochemical parameters of mineral-forming fluids of large ( $\geq 100$  tonnes Au) orogenic gold deposits.

Age, Ma	Temperature, °C	Salinity, wt.% NaCl Equiv	n	Pressure, bar	n
Cenozoic	255	3.7	58	1335	17
0–65	(140–424)	(0.5–14.6)		(500–3400)	
Mesozoic	277	5.8	585	1220	206
65–252	(80–515)	(0.01–37.5)		(190–3380)	
Paleozoic	280	7.7	342	1590	133
252–540	(80–550)	(0.2–28.3)		(150–3460)	
Meso- and Neoproterozoic	275	14.2	51	1200	54
540–1600	(143–454)	(1.0–50.0)		(120–3900)	
Paleoproterozoic	221	13.2	89	1500	5
1600–2500	(48–510)	(0.5–62.4)		(1250–2800)	
Meso-Neoarchean	280	7.0	69	2100	49
2500–3200	(60–462)	(0.1–49.8)		(700–6400)	

n: Number of determinations; Minimum and maximum values are shown in parentheses.

The histograms of the fluid homogenization temperatures (Figure 3) are unimodal, which also indicates that the dataset is homogeneous. They also show that the temperature range of homogenization temperatures widens from the younger to older deposits.

Fluid salinity (Figure 4) are also shows unimodal distribution. The histograms for the Meso- and Neoarchean and Neoproterozoic show a very weak tendency toward bimodality, but the sets of data on these deposits are the smallest, and hence, the bimodality of these diagrams may be explained simply by the scarcity of the data in each of the sets. The salinity range generally widens with increasing age of the fluids, as also do the maximum salinity values. The histograms are skewed, with the maxima occurring in the regions of the minimum salinity values.

The pressure histograms (Figure 5) are generally also skewed unimodal, with maxima within the range of 500–2000 bar. Data on the Precambrian deposits are obviously scarcer than those on Phanerozoic ones. The maximum pressure values generally tend to increase from the younger to older deposits, which widens the range of the pressure values.

The boxplot diagrams provide more information for analysis of the distribution because they display the region in which half of the values plot and the maximum and minimum parameters, outliers, and the median and average values. For the temperature (Figure 6), most of the determined values obviously lie within the range of 200 to 300 °C. The medians, Q25 (first quartile), Q75 (third quartile), and the maximum homogenization temperature values slightly increase from the Cenozoic to Paleozoic. Simultaneously the ranges of the maximum and minimum values widen. No such tendencies were detected for the Precambrian fluids, but the ranges of all of the boundary values are similar. We detected small outliers only for the data on the Mesozoic and Paleozoic, which indicates that the whole dataset is homogeneous. The facts presented above seem to indicate that the orogenic fluid systems are thermostated, perhaps, because of their flow-through character.

The boxplot diagram for the salinity values (Figure 7) shows that most of these values group in the range of moderate concentrations and do not exceed 18 wt.%. However, the overall range of the concentrations is roughly twice as large, and some outliers correspond to even greater salinity values. It is interesting that the salinity values statistically significantly increase with increasing age of the deposits. This is seen in the monotonous increase in the median values, Q75, the maximum ranges, and the maximum outliers. The overall tendencies are slightly disturbed by data on the Meso- and Neoproterozoic, which define a local maximum, and by data of the Meso- and Neoarchean, which define a local minimum. However, as was mentioned above, these time periods are characterized by the smallest amounts of data. The deviations from the general tendency may be explained simply by the insufficiency of the factual material.

The boxplot diagram for the fluid pressures (Figure 8) shows that most of the pressure values almost do not vary and group within the range of 500 to 2500 bar. However, comparison of the maximum variation ranges and the maximum outliers shows a general increase in these parameters with increasing age of the deposits. The general tendency is slightly disturbed by data on the Meso- and Neoproterozoic and on the Meso- and Neoarchean, which define a local minimum. However, these time spans are characterized by scarce data (see above). The same conclusion is derived from the analysis of the median pressure values.

The results of the calculation of Student's t-test for comparing the average values of fluid salinity and pressure, performed in pairs for all combinations, showed statistically significant differences between all samples under consideration. Below for an example are the results of an independent-samples Student's t-test for comparison of characteristics of Cenozoic and Paleoproterozoic fluids. The significant difference was revealed between the scores of salinity values for Cenozoic and Paleoproterozoic fluids: mean value  $M = 4.29$  wt.%, standard deviation  $SD = 0.168$  and  $M = 9.208$  wt.%,  $SD = 0.395$ , respectively; Student t-test for this pair  $t(771) = 11.47$ , and significance  $p = 0.00000$ . The obtained t value is significantly higher than the critical value of the Student t-test, which is 1.972, at a significance level of  $\alpha = 0.05$ . These results show that the difference in Cenozoic and Paleoproterozoic average salinity values is statistically significant.

An analogous calculation was performed to compare values of pressure of Cenozoic and Paleoproterozoic fluids. The significant difference also was found in the scores of pressure values for Cenozoic and Paleoproterozoic fluids ( $M = 1380$  bar,  $SD = 77.75$ ) and ( $M = 2577$  bar,  $SD = 187.50$ ), respectively;  $t(161) = 5.90$ ,  $p = 0.00000$ . The obtained  $t$  value, as in the previous case, greatly exceeds the critical value of the Student's  $t$ -test, which is equal to 1.975, at a significance level  $\alpha = 0.05$ . This proves that the differences in the mean pressures of the Cenozoic and Paleoproterozoic fluids are statistically significant.

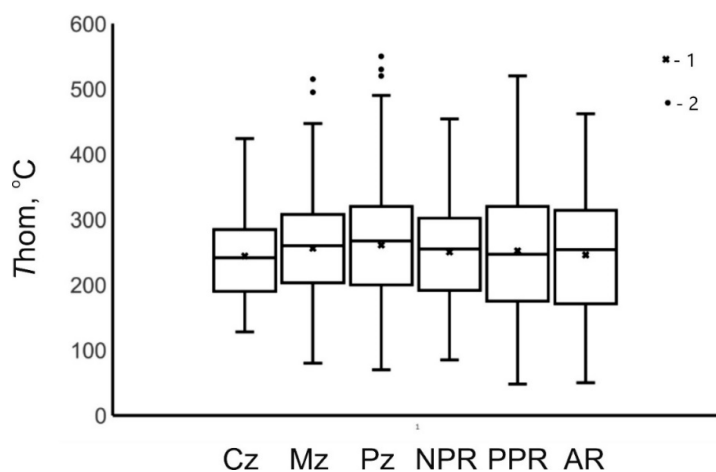


**Figure 6.** Boxplot diagrams for the temperatures of the mineralizing fluids of orogenic gold deposits of various age. Here and in Figures 7 and 8: Cz—Cenozoic; Mz—Mesozoic; Pz—Paleozoic; NPR—Meso- and Neoproterozoic, Paleoproterozoic; AR—Meso-Neoarchean; 1—average; 2—outliers.

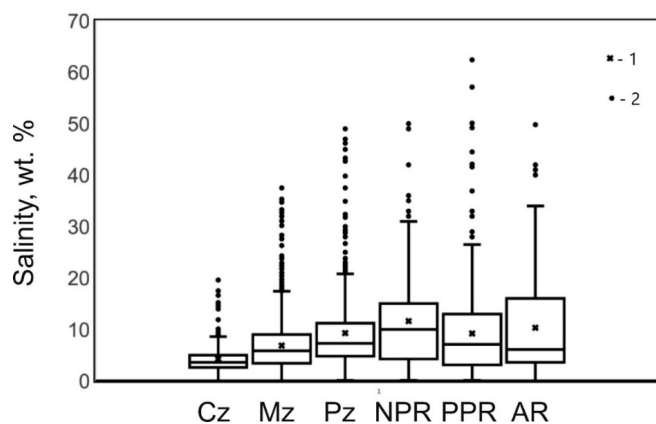


**Figure 7.** Boxplot diagrams for the salinity of the mineralizing fluids of orogenic gold deposits of various age.

We did not detect any differences in the parameters of fluids from the large deposits relative to those from the smaller ones (Table 9).

In considering information not shown in the diagrams but discussed in literature following three types of fluid can be distinguished: (1) heterogeneous fluid, which is mixture of dense gaseous fluid and liquid aqueous salt fluid; (2) homogeneous aqueous salt fluid; and (3) homogeneous dense gaseous fluid, which can contain variable proportions of  $\text{CO}_2$ ,  $\text{CH}_4$ , and  $\text{N}_2$ . The phase composition of the fluids seems to also correlate with the age. The fluids at the young deposits correspond to types (1) and (2), whereas fluids at the Precambrian deposits can be of any of the three type.

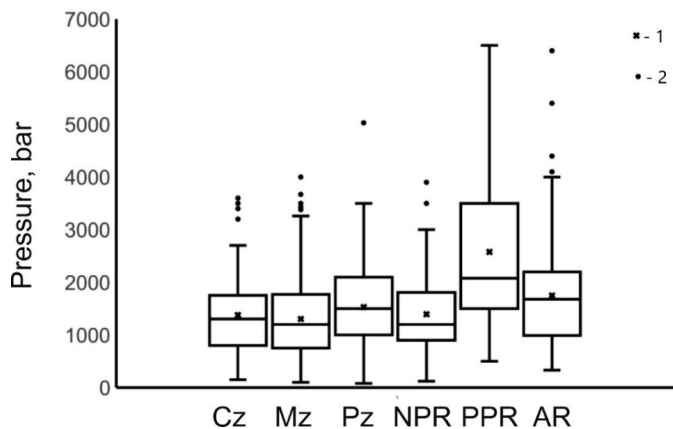


**Figure 8.** Boxplot diagrams for the pressure of the mineralizing fluids of orogenic gold deposits of various age.

Orogenic gold deposits are major exploration targets and global gold producers, and are thus actively studied using various microanalytical techniques. In addition to hundreds of papers on the fluid regime of individuals gold deposits, three significant reviews have been published on fluid inclusion features of orogenic gold deposits worldwide [4,192,193].

A principal conclusion formulated by [192] can be summarized as that orogenic gold deposits are produced from heterogeneous fluids consisting of a high-density gas phase, dominantly CO<sub>2</sub>, and an aqueous solution with relatively low salt concentrations. This conclusion generally does not contradict our analysis and most of the orogenic gold deposits evaluated here some 20 years later continue to show these features. However, a notable number of the deposits were formed from a homogeneous fluid. Moreover, some orogenic gold deposits were generated from chloride brines (e.g., Gara and Yalea, Mali; Telfer, Australia; Irokinda, Russia). This provides evidence to argue that a heterogeneous ore-forming fluid and a low salinity may not necessarily be inherent to fluids required to form orogenic gold deposits.

Another review [4] is even more extensive, but the principal conclusions remain the same. This review suggests that trapped chlorine brines these are low-temperature fluid inclusions that are not related to the ore-forming process but rather reflect the influx of pore water solutions into the hydrothermal system. Based on our comprehensive review of the existing literature, we argue that fluid inclusions with high-temperature chloride brines documented at some of the deposits (Gara and Yalea, Mali; Telfer, Australia; Irokinda, Russia; etc.) were trapped when the host quartz crystallized simultaneously with the native gold. These more saline ore fluids are also not equally observed in deposits of different ages but appear to be significant only during certain epochs. It is also reasonable to suggest that the ability of fluid at orogenic gold deposits to carry gold only insignificantly depends on the chemical composition of this fluid. Indeed, both chloride and hydrocarbonate (containing CO<sub>2</sub> and CH<sub>4</sub>) fluids were found in variable proportions (up to the dominance of either the oxidized or the reduced species) at the deposits.

Key-idea idea stressed throughout the third review [193] is that the composition of the inclusions may have changed during the post-mineral history of the mineralization, when the deposits were exhumed. These changes may reflect both post-entrapment modifications of fluid inclusions (e.g., necking, leackage, etc.) or overprinting by of later generations of secondary inclusions during the exhumation. This is an important conclusion, which undoubtedly requires consideration for a meaningful interpretation of fluid inclusion data. However, the more reliable publications on fluid inclusions, to which our review is devoted, soundly demonstrate compiled data reflect the ore-forming process. It is thus reasonable to suggest that the evaluated parameters here do pertain to the origin of the gold ores and not to post-ore processes. The other important conclusion that follows from analysis

of the paper by [194], which reviews both data on fluid inclusions and stable isotopes, is that the orogenic gold ore-forming fluids may have originated from more than one crustal source reservoir.

Our data generally do not contradict earlier reviews [4,192,193] and slightly append them. At the same time, the detected statistically significant differences in some parameters of mineralizing fluids at orogenic gold deposits of different age is principally new information, which deserves adequate understanding.

We think that it is hardly probable that similar hydrothermal processes that produced deposits of the same genetic type could principally change through the Earth's history. Analysis of geological descriptions in all of the publications indicates that there were no cardinal differences between the geological structures of orogenic deposits formed at different time. These are commonly vein- or stringer-hosted gold mineralization in sedimentary or metamorphic rocks. The metamorphic rocks are usually metamorphosed to the greenschist or, sometimes (for the Archean deposits) amphibolite facies.

To understand the trends and relations described above, one has to recall that orogenic fluid systems operate within a broad range of depths: from a few to 25 km [1,2], and the deposits are now variably exhumed and eroded. This is in good agreement with the current model of orogenic gold deposits (Figure 9) [194]. The depths of erosion of younger deposits are, in general, shallower than those of older deposits, as was demonstrated using extensive information in [195], a paper aimed to explain why there are no ancient epithermal deposits. Epithermal deposits are formed at shallow depths, whereas orogenic deposits were produced at much greater ones. Because of this, most Cenozoic gold deposits occur at various depths, and only some of them are exposed by erosion in areas of young orogenic processes (for example, in Tibet). The older an orogenic gold deposit, the greater depth of its erosion. Archean deposits in India are eroded to the greatest depths and are the world's deepest orogenic gold deposits ("hypozonal" according to [194]). Fluid pressures higher than 6 kbar were detected at these deposits [165]. In addition, one shall keep in mind that our statistical analysis of fluid parameters was carried out for fairly long-time spans. The depths of erosion of the deposits of each of the age groups can thus significantly vary and, hence, also affect the scatter of parameters within the groups. Because of this, statistically significant values in the boxplots are not the maximum parameters in the ranges but also outliers.

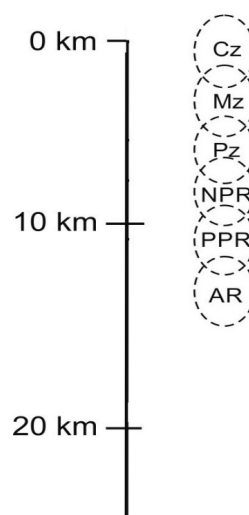


**Figure 9.** The average levels of exhumation of orogenic gold deposits of different ages.

There can be different reasons for the increase in the salinity of fluids at orogenic deposits with depth. It is pertinent to recall that deep crustal high-temperature and high-pressure zones typically host chloride brines as pore waters [196]. This sheds light on why they are recognized in the deeper parts of orogenic gold fluid systems, as is reflected in the occurrence of brine-bearing fluid inclusions in the older gold deposits. At shallower levels, the systems may also undergo input of less mineralized

fluids of a different nature. Another possible explanation of the occurrence of high-temperature brines in orogenic fluid systems may be the involvement of magmatic fluids in the mineral-forming processes [153].

We believe that the aforementioned differences we detected between parameters and composition of mineral-forming fluids at orogenic gold deposits reflect the vertical zoning of the mineralizing fluid systems of orogenic gold deposits. This zoning can remain unidentified or ignored when a single deposit is studied, but it becomes quite obvious when the whole ranges of the parameters of such deposits are studied. This zoning has nevertheless never been mentioned before with reference to orogenic mineralizing systems and shall be taken into account when these deposits are studied.

**Supplementary Materials:** The following are available online at <http://www.mdpi.com/2075-163X/10/1/50/s1>.

**Author Contributions:** V.Y.P.—the idea of the article, the grouping of deposits by the time of their formation, statistical processing and writing of the text. V.B.N.—browse the literature, select the necessary publications, fill out the database. All authors have read and agreed to the published version of the manuscript.

**Funding:** This research was funded by Program no. 48 of the Russian Academy of Sciences and the Scientific Program of IGEM RAS.

**Acknowledgments:** The authors would like to thank Richard Goldfarb for his assistance in the expert evaluation of the types of gold deposits.

**Conflicts of Interest:** The authors declare no conflict of interest.

## References

1. Groves, D.I.; Goldfarb, R.J.; Gebre-Mariam, M.; Hagemann, S.G.; Robert, F. Orogenic gold deposits: A proposed classification in the context of their crustal distribution and relationship to other gold deposit types. *Ore Geol. Rev.* **1998**, *13*, 7–27. [[CrossRef](#)]
2. Goldfarb, R.J.; Groves, D.I.; Gardoll, S. Orogenic gold and geologic time: A global synthesis. *Ore Geol. Rev.* **2001**, *18*, 1–75. [[CrossRef](#)]
3. Naumov, V.B.; Dorofeeva, V.A.; Mironova, O.F. Principal physicochemical parameters of natural mineral-forming fluids. *Geochem. Intern.* **2009**, *47*, 777–802. [[CrossRef](#)]
4. Goldfarb, R.J.; Groves, D.I. Orogenic gold: Common or evolving fluid and metal sources through time. *Lithos* **2015**, *233*, 2–26. [[CrossRef](#)]
5. Goldfarb, R.J.; Taylor, R.D.; Collins, G.S.; Goryachev, N.A.; Orlandini, O.F. Phanerozoic continental growth and gold metallogeny of Asia. *Gondwana Res.* **2014**, *25*, 48–102. [[CrossRef](#)]
6. Goldfarb, R.J.; Leach, D.L.; Miller, M.L.; Pickthorn, W.J. Geology, metamorphic setting, and genetic constraints of epigenetic lode-gold mineralization within the Cretaceous Valdez Group, south-central Alaska. *Turbid. Hosted Gold Depos. Geol. Assoc. Can. Spec. Pap.* **1986**, *32*, 87–105.
7. Walton, L.A. Geology and Geochemistry of the Venus Au–Ag–Pb–Zn Deposit, Yukon Territory. Master’s Thesis, The University of Alberta, Edmonton, AB, Canada, 7 May 1987.
8. Lattanzi, P.F.; Curti, E.; Bastogi, M. Fluid inclusions studies on the gold deposits on the upper anzasca Valley, northwestern alps, Italy. *Econ. Geol.* **1989**, *84*, 1382–1397. [[CrossRef](#)]
9. Zhang, X.; Nesbitt, B.E.; Muehlenbachs, K. Gold mineralization in the Okanagan Valley, southern British Columbia: Fluid inclusion and stable isotope studies. *Econ. Geol.* **1989**, *84*, 410–424. [[CrossRef](#)]
10. Goldfarb, R.J.; Leach, D.L.; Rose, S.C.; Landis, G.P. Fluid inclusion geochemistry of gold-bearing quartz veins of the Juneau gold belt, southeastern Alaska—Implications for ore genesis. *Econ. Geol. Monogr.* **1989**, *6*, 363–375.
11. Leitch, C.H.B. Geology, Wallrock Alteration, and Characteristic of the Ore Fluid at the Bralorne Mesothermal Gold Vein Deposit, Southwester British Columbia. Ph.D. Thesis, The University of British Columbia, Vancouver, BC, Canada, 25 April 1989.
12. Diamond, L.W. Fluid inclusions evidence for P–V–T–X evolution hydrothermal solutions in late-alpine gold-quartz veins at Brusson, Val d’Ayas, Northwest Italian Alps. *Am. J. Sci.* **1990**, *290*, 912–958. [[CrossRef](#)]
13. Leitch, C.H.B.; Godwin, C.I.; Brown, T.H.; Taylor, B.E. Geochemistry of mineralizing fluids in the Bralorne-Pioneer mesothermal gold vein deposit, British Columbia, Canada. *Econ. Geol.* **1991**, *86*, 318–353. [[CrossRef](#)]

14. Craw, D. Fluid evolution, fluid immiscibility and gold deposition during Cretaceous-Recent tectonics and uplift of the Otago and Alpine Schist, New Zealand. *Chem. Geol.* **1992**, *98*, 221–236. [[CrossRef](#)]
15. Craw, D.; Teagle, D.A.H.; Belocky, R. Fluid immiscibility in Late-Alpine gold-bearing veins, Eastern and Northwestern European Alps. *Miner. Depos.* **1993**, *28*, 28–36. [[CrossRef](#)]
16. Miller, L.D.; Goldfarb, R.J.; Snee, L.W.; Cent, C.A.; Kirkham, R.A. Structural geology, age, and mechanisms of gold vein formation at the Kensington and Jualin deposits, Berners Bay district, southeast Alaska. *Econ. Geol.* **1995**, *90*, 343–368. [[CrossRef](#)]
17. Li, G.M.; Qin, K.Z.; Ding, K.S.; Liu, T.B.; Li, J.X.; Wang, S.H.; Jiang, S.Y.; Zhang, X.C. Geology, Ar–Ar age and mineral assemblage of Eocene Skarn Cu–Au ± Mo deposits in the southeastern gangdese arc, southern tibet: Implications for deep exploration. *Resour. Geol.* **2006**, *56*, 315–336. [[CrossRef](#)]
18. Moritz, R.; Ghasban, F.; Singer, B.S. Eocene gold ore formation at muteh, sanandaj-sirjan tectonic zone, western iran: A result of late-stage extension and exhumation of metamorphic basement rocks within the zagros orogen. *Econ. Geol.* **2006**, *101*, 1497–1524. [[CrossRef](#)]
19. Kekelia, S.A.; Kekelia, M.A.; Kuloshvili, S.I.; Sadradze, N.G.; Gagnidze, N.E.; Yaroshevich, V.Z.; Asatiani, G.G.; Doebrich, J.L.; Goldfarb, R.J.; Marsh, E.E. Gold deposits and occurrences of the greater caucasus, georgia republic: Their genesis and prospecting criteria. *Ore Geol. Rev.* **2008**, *34*, 369–386. [[CrossRef](#)]
20. Ruiz, F.J.Q. La Herradura ore deposit: An orogenic gold deposit in Northwestern Mexico. Master’s Thesis, University of Arisona, Tucson, AZ, USA, 4 May 2008.
21. Sun, X.M.; Zhang, Y.; Xiong, D.X.; Sun, W.D.; Shi, G.Y.; Zhai, W.; Wang, S.W. Crust and mantle contributions to gold-forming process at the dapeng deposit, ailaoshan gold belt, Yunnan, China. *Ore Geol. Rev.* **2009**, *36*, 235–249. [[CrossRef](#)]
22. Jiang, S.H.; Nie, F.J.; Hu, P.; Lai, X.R.; Liu, Y.F. Mayum: An orogenic gold deposit in Tibet, China. *Ore Geol. Rev.* **2009**, *36*, 160–173. [[CrossRef](#)]
23. Zhai, W.; Suna, X.; Yi, J.; Zhang, X.; Mo, R.; Zhou, F.; Wei, H.; Zeng, Q. Geology, geochemistry, and genesis of orogenic gold—Antimony mineralization in the Himalayan Orogen, South Tibet, China. *Ore Geol. Rev.* **2014**, *58*, 68–90. [[CrossRef](#)]
24. Taghipour, B.; Ahmadnejad, F. Geological and geochemical implications of the genesis of the qolqoleh orogenic gold mineralisation, Kurdistan Province (Iran). *Geologos* **2015**, *21*, 31–57. [[CrossRef](#)]
25. Sun, X.; Wei, H.; Zhai, W.; Shi, G.; Liang, Y.; Mo, R.; Han, M.; Yi, J.; Zhang, X. Fluid inclusion geochemistry and Ar–Ar geochronology of the Cenozoic Bangbu orogenic gold deposit, southern Tibet, China. *Ore Geol. Rev.* **2016**, *74*, 196–210. [[CrossRef](#)]
26. Coveney, R.M., Jr. Gold quartz veins and auriferous granite at the oriental mine, alleghany district, California. *Econ. Geol.* **1981**, *76*, 2176–2199. [[CrossRef](#)]
27. Read, J.J.; Meinert, L.D. Gold-bearing quartz vein mineralization at the big hurrah mine, Seward Peninsula, Alaska. *Econ. Geol.* **1986**, *81*, 1760–1774. [[CrossRef](#)]
28. Weir, R.H., Jr.; Kerrick, D.M. Mineralogic, fluid inclusion, and stable isotope studies of several gold mines in the mother lode, Tuolumne and Mariposa Counties, California. *Econ. Geol.* **1987**, *82*, 328–344. [[CrossRef](#)]
29. Cunningham, C.G.; Ashley, R.P.; Chou, I.-M.; Zushu, H.; Chaoyuan, W.; Wenkang, L. Newly discovered sedimentary rock-hosted disseminated gold deposits in the People’s Republic of China. *Econ. Geol.* **1988**, *83*, 1462–1467. [[CrossRef](#)]
30. So, C.-S.; Yun, S.-T.; Choi, S.-H.; Shelton, K.L. Geochemical studies of hydrothermal gold–silver deposits, Republic of Korea: Youngdong mining district. *Min. Geol.* **1989**, *39*, 9–19.
31. Elder, D.; Cashman, S.M. Tectonic control and fluid evolution in the Quartz Hill, California, lode gold deposit. *Econ. Geol.* **1992**, *87*, 1795–1812. [[CrossRef](#)]
32. Rushton, R.W.; Nesbitt, B.E.; Muehlenbachs, K.; Mortensen, J.K. A fluid inclusion and stable isotope study of Au quartz veins in the klondike district, Yukon Territory, Canada: A section through a mesothermal vein system. *Econ. Geol.* **1993**, *88*, 647–678. [[CrossRef](#)]
33. So, C.-S.; Yun, S.-T.; Sheiton, K.L. Mesothermal gold vein mineralization of the Samdong mine, Youngdong mining district, Republic of Korea. A geochemical and fluid inclusion study. *Miner. Depos.* **1995**, *30*, 384–396. [[CrossRef](#)]
34. Presnell, R.D.; Parry, W.T. Geology and geochemistry of the Barneys canyon gold deposit, Utah. *Econ. Geol.* **1996**, *91*, 273–288. [[CrossRef](#)]

35. Goldfarb, R.J.; Miller, L.D.; Leach, D.L.; Snee, L.W. Gold deposits in metamorphic rocks of Alaska. *Econ. Geol. Monogr.* **1997**, *9*, 151–190.
36. Nie, F.J. Geology and origin of the dongping alkalic-type gold deposit, northern Hebei province, People's Republic of China. *Resour. Geol.* **1998**, *48*, 139–158. [[CrossRef](#)]
37. Yao, Y.; Morteani, G.; Trumbull, R.B. Fluid inclusion microthermometry and the P-T evolution of gold-bearing hydrothermal fluids in the Niuxinshan gold deposit, eastern Hebei province, NE China. *Miner. Depos.* **1999**, *34*, 348–365. [[CrossRef](#)]
38. Mao, J.W.; Zhang, Z.H.; Yang, J.M.; Zhang, Z.C. The Hanshan gold deposit in the Caledonian North Qilian orogenic belt, NW China. *Miner. Depos.* **2000**, *35*, 63–71.
39. Naumov, E.A.; Borovikov, A.A.; Borisenko, A.S.; Zadorozhnyy, M.V.; Murzin, V.V. Physicochemical conditions of formations of epithermal gold–mercury deposits. *Russ. Geol. Geophys.* **2002**, *43*, 1055–1064.
40. Zhong, H.R.; Chao, S.W.; Wu, B.X.; Zhi, T.G.; Hofstra, A.H. Geology and geochemistry of carlin-type gold deposits in China. *Miner. Depos.* **2002**, *37*, 378–392. [[CrossRef](#)]
41. Cheong, S. Fluid inclusion study of metamorphic gold–quartz veins in northwestern Nevada, U.S.A.: Characteristics of tectonically induced fluid. *Geosci. J.* **2002**, *6*, 103–115. [[CrossRef](#)]
42. Mao, J.; Kerrich, R.; Li, H.; Li, Y. High  $^3\text{He}/^4\text{He}$  ratios in the Wangu gold deposit, Hunan province, China: Implications for mantle fluids along the tanlu deep fault zone. *Geochem. J.* **2003**, *36*, 197–208. [[CrossRef](#)]
43. Cromie, P.W.; Zaw, K. Geological setting, nature of ore fluids and sulphur isotope geochemistry of the Fu Ning Carlin-type gold deposits, Yunnan Province, China. *Geofluids* **2003**, *3*, 133–143. [[CrossRef](#)]
44. Fan, H.R.; Zhai, M.G.; Xie, Y.H.; Yang, J.H. Ore-forming fluids associated with granite-hosted gold mineralization at the Sanshandao deposit, Jiaodong gold province, China. *Miner. Depos.* **2003**, *38*, 739–750. [[CrossRef](#)]
45. Mao, J.; Li, Y.; Goldfarb, R.; He, Y.; Zaw, K. Fluid inclusion and noble gas studies of the dongping gold deposit, Hebei Province, China: A mantle connection for mineralization? *Econ. Geol.* **2003**, *98*, 517–534. [[CrossRef](#)]
46. Goldfarb, R.J.; Ayuso, R.; Miller, M.L.; Ebert, S.W.; Marsh, E.E.; Petsel, S.A.; Miller, L.D.; Bradley, D.; Johnson, C.; McClelland, W. The late cretaceous donlin creek gold deposit, Southwestern Alaska: Controls on epizonal ore formation. *Econ. Geol.* **2004**, *99*, 643–671. [[CrossRef](#)]
47. Bortnikov, N.S.; Bryzgalov, I.A.; Krivitskaya, N.N.; Prokofiev, V.Y.; Vikentieva, O.V. The Maiskoe multimegastage disseminated gold–sulfide deposit (Chukotka, Russia): Mineralogy, fluid inclusions, stable isotopes (O and S), history, and conditions of formation. *Geol. Ore Depos.* **2004**, *46*, 409–440.
48. Li, Y.G.; Zhai, M.G.; Miao, L.C.; Xue, L.W.; Zhu, J.W.; Guan, H. Ore-forming fluids of the anjiayingzi gold deposit in Chifeng region, Inner Mongolia. *Acta Petrol. Sin.* **2004**, *20*, 961–968.
49. Zhang, X.H.; Liu, Q.; Ma, Y.J.; Wang, H. Geology, fluid inclusions, isotope geochemistry, and geochronology of the Paishanlou shear zone-hosted gold deposit, North China Craton. *Ore Geol. Rev.* **2005**, *26*, 325–348. [[CrossRef](#)]
50. Zeng, Q.; Liu, J.; Liu, H.; Shen, P.; Zhang, L. The Ore-forming Fluid of the Gold Deposits of Muru Gold Belt in Eastern Shandong, China—A case study of denggezhuang gold deposit. *Resour. Geol.* **2006**, *56*, 375–384. [[CrossRef](#)]
51. Yoo, B.C.; Lee, H.K.; White, N.C. Gold-bearing mesothermal veins from the gubong mine, cheongyang gold district, Republic of Korea: Fluid inclusion and stable isotope studies. *Econ. Geol.* **2006**, *101*, 883–901. [[CrossRef](#)]
52. Hu, F.-F.; Fan, H.-R.; Zhai, M.-G.; Jin, C.-W. Fluid evolution in the rushan lode gold deposit of Jiaodong Peninsula, eastern China. *J. Geochem. Explor.* **2006**, *89*, 161–164. [[CrossRef](#)]
53. Li, X.F.; Mao, J.W.; Wang, C.; Watanabe, Y. The Daduhe gold field at the eastern margin of the Tibetan Plateau: He, Ar, S, O, and hisotopic data and their metallogenetic implications. *Ore Geol. Rev.* **2007**, *30*, 244–256. [[CrossRef](#)]
54. Bortnikov, N.S.; Gamyanin, G.N.; Vikent'eva, O.V.; Prokofiev, V.Y.; Alpatov, V.A.; Bakharev, A.G. Fluid composition and origin in the hydrothermal system of the nezhdaninsky gold deposit, Sakha (Yakutia), Russia. *Geol. Ore Depos.* **2007**, *49*, 87–128. [[CrossRef](#)]
55. Zhang, Z.Q.; Yong, L.; Chen, Y.J. Fluid inclusion study of the Linglong gold deposit, Shandong province, China. *Acta Petrol. Sin.* **2007**, *23*, 2207–2216.

56. Obolensky, A.A.; Gushchina, L.V.; Borisenko, A.S.; Borovikov, A.A.; Pavlova, G.G. Antimony in hydrothermal processes: Solubility, conditions of transfer, and metal-bearing capacity of solutions. *Russ. Geol. Geophys.* **2007**, *48*, 992–1001. [[CrossRef](#)]
57. Gamyanin, G.N.; Prokofiev, V.Y.; Goryachev, N.A.; Bortnikov, N.S. Fluid inclusions in quartz of sin-granitic precious metals deposit of north-earth of Russia. In *Part of Mineralogy in Knowledge of Ore-Forming Processes*; Institut Geologii Rudnykh Mestorozhdeniy, Petrografii, Mineralogii I Geokhimii Ran (IGEM RAS): Moscow, Russia, 2007; pp. 92–97.
58. Aristov, V.V.; Konstantiov, M.M.; Kryazhev, S.G. Genetic features of gold and silver deposits from the Western Verkhoyansk area: Fluid inclusion and isotope data. *Geochem. Intern.* **2008**, *46*, 313–317. [[CrossRef](#)]
59. Goryachev, N.A.; Vikent'eva, O.V.; Bortnikov, N.S.; Prokofiev, V.Y.; Alpatov, V.A.; Golub, V.V. The world-class natalka gold deposit, Northeast Russia: REE patterns, fluid inclusions, stable oxygen isotopes, and formation conditions of ore. *Geol. Ore Depos.* **2008**, *50*, 362–390. [[CrossRef](#)]
60. Volkov, A.V.; Sidorov, V.A.; Prokofiev, V.Y.; Sidorov, A.A. Polychronous formation of the rodionovskoe gold-quartz deposit, Russian northeast. *Dokl. Earth Sci.* **2009**, *424*, 19–23. [[CrossRef](#)]
61. Su, W.; Heinrich, C.A.; Pettke, T.; Zhang, X.; Hu, R.; Xia, B. Sediment-hosted gold deposits in Guizhou, China: Products of wall-rock sulphidation by deep crustal fluids. *Econ. Geol.* **2009**, *104*, 73–93. [[CrossRef](#)]
62. Yoo, B.C.; Lee, H.K.; White, N.C. Mineralogical, fluid inclusion, and stable isotope constraints on mechanisms of ore deposition at the Samgwang mine (Republic of Korea)—A mesothermal, vein-hosted gold–silver deposit. *Miner. Depos.* **2010**, *45*, 161–187. [[CrossRef](#)]
63. Bortnikov, N.S.; Gamynin, G.N.; Vikent'eva, O.V.; Prokofiev, V.Y.; Prokop'ev, A.V. The sarylakh and sentachan gold–antimony deposits, Sakha-Yakutia: A case of combined mesothermal gold–quartz and epithermal stibnite ore. *Geol. Ore Depos.* **2010**, *52*, 339–372. [[CrossRef](#)]
64. Huang, D.Z.; Wang, X.Y.; Yang, X.Y.; Li, G.M.; Huang, S.Q.; Liu, Z.; Peng, Z.H.; Qiu, R.L. Geochemistry of gold deposits in the zhangbaling tectonic belt, Anhui province, China. *Int. Geol. Rev.* **2011**, *53*, 612–634. [[CrossRef](#)]
65. Volkov, A.V.; Savva, N.E.; Sidorov, A.A.; Prokofiev, V.Y.; Goryachev, N.A.; Voznesensky, S.D.; Al'shevsky, A.V.; Chernova, A.D. Shkol'noe gold deposit, the Russian northeast. *Geol. Ore Depos.* **2011**, *53*, 1–26. [[CrossRef](#)]
66. Obolensky, A.A.; Gushchina, L.V.; Anisimova, G.S.; Serkebaeva, E.S.; Tomilenko, A.A.; Gibsher, N.A. Physicochemical modeling of mineral formation processes at the badran gold deposit (Yakutia). *Russ. Geol. Geophys.* **2011**, *52*, 290–1001. [[CrossRef](#)]
67. Volkov, A.V.; Prokofiev, V.Y.; Alekseev, V.Y.; Baksheev, I.A.; Sidorov, A.A. Ore-forming fluids and conditions of formation of gold–sulfide–quartz mineralization in the shear zone: Pogromnoe deposit (Eastern Transbaikalian Region). *Dokl. Earth Sci.* **2011**, *441*, 1492–1497. [[CrossRef](#)]
68. Zhou, Z.J.; Jiang, S.Y.; Qin, Y.; Zhao, H.X.; Hu, C.J. Fluid inclusion characteristics and ore genesis of the Wenyu gold deposit, Xiaoqinling gold belt. *Acta Petrol. Sin.* **2011**, *27*, 3787–3799.
69. Gu, X.X.; Zhang, Y.M.; Li, B.H.; Dong, S.Y.; Xue, C.J.; Fu, S.H. Hydrocarbon- and ore-bearing basinal fluids: A possible link between gold mineralization and hydrocarbon accumulation in the Youjiang basin, South China. *Miner. Depos.* **2012**, *47*, 663–682. [[CrossRef](#)]
70. Li, J.-W.; Li, Z.-K.; Zhou, M.F.; Chen, L.; Bi, S.-J.; Deng, X.-D.; Qui, H.-N.; Cohen, B.; Selby, D.; Zhao, X.-F. The Early Cretaceous Yangzhaiyu Lode Gold Deposit, North China Craton: A Link Between Craton Reactivation and Gold Veining. *Econ. Geol.* **2012**, *107*, 43–79. [[CrossRef](#)]
71. Tang, K.-F.; Li, J.W.; Selby, D.; Zhou, M.F.; Bi, S.J.; Deng, X.D. Geology, mineralization, and geochronology of the Qianhe gold deposit, Xiong'ershan area, southern North China Craton. *Miner. Depos.* **2013**, *48*, 729–747. [[CrossRef](#)]
72. Hu, F.F.; Fan, H.R.; Jiang, X.H.; Li, X.C.; Yang, K.F.; Mernagh, T. Fluid inclusions at different depths in the Sanshandao gold deposit, Jiaodong Peninsula, China. *Geofluids* **2013**, *13*, 528–541. [[CrossRef](#)]
73. Zhao, C.; Ni, P.; Wang, G.G.; Ding, J.Y.; Chen, H.; Zhao, K.D.; Cai, Y.T.; Xu, Y.F. Geology, fluid inclusion, and isotope constraints on ore genesis of the Neoproterozoic Jinshan orogenic gold deposit, South China. *Geofluids* **2013**, *13*, 506–527. [[CrossRef](#)]
74. Khishgee, C.; Akasaka, M.; Ohira, H.; Sereenen, J. Gold Mineralization of the Gatsuurt Deposit in the North Khentei Gold Belt, Central Northern Mongolia. *Resour. Geol.* **2014**, *64*, 1–16. [[CrossRef](#)]

75. Peng, Y.; Gu, X.; Zhang, Y.; Liu, L.; Wu, C.; Chen, S. Ore-forming process of the Huijiabao gold district, southwestern Guizhou Province, China: Evidence from fluid inclusions and stable isotopes. *J. Asian Earth Sci.* **2014**, *93*, 89–101. [[CrossRef](#)]
76. Zhou, Z.-J.; Chen, Y.-J.; Jiang, S.-Y.; Zhao, H.-X.; Qin, Y.; Hu, C.-J. Geology, geochemistry and ore genesis of the Wenyu gold deposit, Xiaoqinling gold field, Qinling Orogen, southern margin of North China craton. *Ore Geol. Rev.* **2014**, *59*, 1–20. [[CrossRef](#)]
77. Wen, B.J.; Fan, H.R.; Hu, F.F.; Yang, K.F.; Liu, X.; Cai, Y.C.; Sun, Z.F.; Sun, Z.F. The genesis of pegmatite-type molybdenum mineralization in Sanshandao, and their implications for molybdenum deposit in Jiaodong, East China. *Acta Petrol. Sin.* **2015**, *31*, 1002–1014.
78. Gamyantin, G.N.; Vikent’eva, O.V.; Prokofiev, V.Y.; Bortnikov, N.S. Arkachan: A new gold–bismuth–siderite–sulfide type of deposits in the west verkhoyansky tin district, Yakutia. *Geol. Ore Depos.* **2015**, *57*, 465–495. [[CrossRef](#)]
79. Salvioli-Mariani, E.; Toscani, L.; Boschetti, T.; Bersani, D.; Mattioli, M. Gold mineralisations in the Canan area, lepaguare district, east-central honduras: Fluid inclusions and geochemical constraints on gold deposition. *J. Geochem. Explor.* **2015**, *158*, 243–256. [[CrossRef](#)]
80. Liu, J.; Dai, H.; Zhai, D.; Wang, J.; Wang, Y.; Yang, L.; Mao, G.; Liu, X.; Liao, Y.; Yu, C.; et al. Geological and geochemical characteristics and formation mechanisms of the Zhaishang Carlin-like type gold deposit, western Qinling Mountains, China. *Ore Geol. Rev.* **2015**, *64*, 273–298. [[CrossRef](#)]
81. Zhou, Z.; Chen, Y.-J.; Jiang, S.-Y.; Hu, C.-J.; Qin, Y.; Zhao, H.-X. Isotope and fluid inclusion geochemistry and genesis of the Qiangma gold deposit, Xiaoqinling gold field, Qinling Orogen, China. *Ore Geol. Rev.* **2015**, *66*, 47–64. [[CrossRef](#)]
82. Wen, B.-J.; Fan, H.-R.; Santosh, M.; Hu, F.-F.; Pirajno, F.; Yang, K.-F. Genesis of two different types of gold mineralization in the Linglong gold field, China: Constraints from geology, fluid inclusions and stable isotope. *Ore Geol. Rev.* **2015**, *65*, 643–658. [[CrossRef](#)]
83. Li, L.; Sun, J.-G.; Men, L.-J.; Chai, P. Origin and evolution of the ore-forming fluids of the Erdaogou and Xiaobeigou gold deposits, Jiapigou gold province, NE China. *J. Asian Earth Sci.* **2016**, *129*, 170–190. [[CrossRef](#)]
84. Wen, B.-J.; Fan, H.-R.; Hu, F.-F.; Liu, X.; Yang, K.-F.; Sun, Z.-F. Fluid evolution and ore genesis of the giant Sanshandao gold deposit, Jiaodong gold province, China: Constraints from geology, fluid inclusions and H–O–S–He–Ar isotopic compositions. *J. Geochem. Explor.* **2016**, *171*, 96–112. [[CrossRef](#)]
85. Fu, L.; Wei, J.; Chen, H.; Bagas, L.; Tan, J.; Li, H.; Zhang, D.; Tian, N. The relationship between gold mineralization, exhumation of metamorphic core complex and magma cooling: Formation of the Anjiayingzi Au deposit, northern North China Craton. *Ore Geol. Rev.* **2016**, *73*, 222–240. [[CrossRef](#)]
86. Chai, P.; Sun, J.-G.; Hou, Z.-Q.; Xing, S.-W.; Wang, Z.-Y. Geological, fluid inclusion, H–O–S–Pb isotope, and Ar–Ar geochronology constraints on the genesis of the Nancha gold deposit, southern Jilin Province, northeast China. *Ore Geol. Rev.* **2016**, *72*, 1053–1071. [[CrossRef](#)]
87. Yang, L.-Q.; Deng, J.; Guo, L.-N.; Wang, Z.-L.; Li, X.-Z.; Li, J.-L. Origin and evolution of ore fluid, and gold-deposition processes at the giant Taishang gold deposit, Jiaodong Peninsula, eastern China. *Ore Geol. Rev.* **2016**, *72*, 585–602. [[CrossRef](#)]
88. Song, Y.; Jiang, S.-H.; Bagas, L.; Li, C.; Hu, J.-Z.; Zhang, Q.; Zhou, W.; Ding, H.-Y. The geology and geochemistry of Jinchangyu gold deposit, North China Craton: Implications for metallogenesis and geodynamic setting. *Ore Geol. Rev.* **2016**, *73*, 313–329. [[CrossRef](#)]
89. Zheng, Y.; Zhou, Y.; Wang, Y.; Shen, W.; Yang, Z.; Li, X.; Xiao, F. A fluid inclusion study of the Hetai goldfield in the Qinzhou Bay–Hangzhou Bay metallogenic belt, South China. *Ore Geol. Rev.* **2016**, *73*, 346–353. [[CrossRef](#)]
90. Ma, Y.; Xiong, S.-F.; Li, H.-L.; Jiang, S.-Y. Origin and evolution of the ore-forming fluids in the Liyuan gold deposit, central North China Craton: Constraints from fluid inclusions and H–O–C isotopic compositions. *Geofluids* **2017**, *6*, 1–21. [[CrossRef](#)]
91. Xu, D.; Wang, Z.; Wu, C.; Zhou, Y.; Shan, Q.; Hou, M.; Fu, Y.; Zhang, X. Mesozoic gold mineralization in Hainan Province of South China: Genetic types, geological characteristics and geodynamic settings. *J. Asian Earth Sci.* **2017**, *137*, 80–108. [[CrossRef](#)]
92. Gao, S.; Xu, H.; Li, S.; Santosh, M.; Zhang, D.; Yang, L.; Quan, S. Hydrothermal alteration and ore-forming fluids associated with gold-tellurium mineralization in the Dongping gold deposit, China. *Ore Geol. Rev.* **2017**, *80*, 166–184. [[CrossRef](#)]

93. Liu, J.; Wang, J.; Liu, Y.; Tian, J.; Li, X.; Zhang, H. Ore genesis of the Xiadian gold deposit, Jiaodong Peninsula, East China: Information from fluid inclusions and mineralization. *Geol. J.* **2017**, *53*, 1–19. [CrossRef]
94. Guo, L.-N.; Goldfarb, R.J.; Wang, Z.-L.; Li, R.-H.; Chen, B.-H.; Li, J.-L. A comparison of Jiaojaia- and Linglong-type gold deposit ore-forming fluids: Do they differ? *Ore Geol. Rev.* **2017**, *88*, 511–533. [CrossRef]
95. Xu, D.; Deng, T.; Chi, G.; Wang, Z.; Zou, F.; Zhang, J.; Zou, S. Gold mineralization in the Jiangnan Orogenic Belt of South China: Geological, geochemical and geochronological characteristics, ore deposit-type and geodynamic setting. *Ore Geol. Rev.* **2017**, *88*, 565–618. [CrossRef]
96. Seccombe, P.K.; Hicks, M.N. The Hill End goldfield, NSW, Australia—Early metamorphic deposition of auriferous quartz veins. *Mineral. Petrol.* **1989**, *40*, 257–273. [CrossRef]
97. Bril, H.; Beaufort, D. Hydrothermal alteration and fluid circulation related to W, Au, and Sb vein mineralizations, Haut Allier, Massif Central, France. *Econ. Geol.* **1989**, *84*, 2237–2251. [CrossRef]
98. Spiridonov, E.M.; Prokofiev, V.Y. Geochemical characteristics and conditions of formation of the plutonogenetic gold–telluride deposits in the caledonides of Northern Kazakhstan. *Int. Geol. Rev.* **1990**, *32*, 188–202. [CrossRef]
99. Peters, S.G.; Golding, S.D.; Dowling, K. Melange- and sediment-hosted gold-bearing quartz veins, Hodgkinson gold field, Queensland, Australia. *Econ. Geol.* **1990**, *85*, 312–327. [CrossRef]
100. Schreiber, D.W.; Fontbote, L.; Lochmann, D. Geologic setting, paragenesis, and physicochemistry of gold quartz veins hosted by plutonic rocks in the Pataz region. *Econ. Geol.* **1990**, *85*, 1328–1347. [CrossRef]
101. Prokofiev, V.Y.; Sanina, N.B. Geochemistry of the mineralizing fluids at the Sarala gold deposit, Kuznetsk Alatau. *Geochem. Intern.* **1992**, *29*, 42–49.
102. Gao, Z.L.; Kwak, T.A.P.; Changkakoti, A.; Hussein, E.; Gray, J. Supergene ore and hypogene nonore mineralization at the Nagambie sediment-hosted gold deposit, Victoria, Australia. *Econ. Geol.* **1995**, *90*, 1747–1763. [CrossRef]
103. Grebenshikova, V.I.; Prokofiev, V.Y.; Troshin, Y.P. New data of formation conditions of gold vein of Kommunar gold deposit (Kuznetsk Alatau). *Dokl. Earth Sci.* **1995**, *340*, 239–242.
104. Bortnikov, N.S.; Prokofiev, V.Y.; Razdolina, N.V. Origin of the charmitan gold–quartz deposit (Uzbekistan). *Geol. Ore Depos.* **1996**, *38*, 208–226.
105. Jia, Y.; Li, X.; Kerrich, R. A fluid inclusion study of Au-bearing quartz vein systems in the Central and North Deborah deposits of the Bendigo gold field, central Victoria, Australia. *Econ. Geol.* **2000**, *95*, 467–493. [CrossRef]
106. Laverov, N.P.; Prokofiev, V.Y.; Distler, V.V.; Spiridonov, A.M.; Yudovskaya, M.A.; Grebenshikova, V.I.; Matel, N.L. New data on conditions of ore deposition and composition of ore-forming fluids in the Sukhoi Log gold–platinum deposit. *Dokl. Earth Sci.* **2000**, *371*, 357–361.
107. Baksheev, I.A.; Prokofiev, V.Y.; Ustinov, V.I. Genesis of metasomatic rocks and mineralized veins at the Berezovskoe deposit, central Urals: Evidence from fluid inclusions and stable isotopes. *Geochem. Intern.* **2001**, *39*, S129.
108. Mernagh, T.P. A fluid inclusion study of the Fosterville mine: A turbidite-hosted gold field in the western Lachlan fold belt, Victoria, Australia. *Chem. Geol.* **2001**, *173*, 91–106. [CrossRef]
109. Bellot, J.-P.; Lerouge, C.; Bailly, L.; Bouchot, V. The biards Sb–Au-bearing shear zone (Massif Central, France): An indicator of crustal-scale transcurrent tectonics guiding late Variscan collapse. *Econ. Geol.* **2003**, *98*, 1427–1447. [CrossRef]
110. Safonov, Y.G.; Volkov, A.V.; Volkson, A.A.; Genkin, A.D.; Krylova, T.L.; Chugayev, A.V. The maisk quartz gold deposit (Northern Karelia): Geological, mineralogical, and geochemical studies and some genetic problems. *Geol. Ore Depos.* **2003**, *45*, 375–394.
111. Giles, A.D.; Marshall, B. Genetic significance of fluid inclusions in the CSA Cu–Pb–Zn deposit, Cobar, Australia. *Ore Geol. Rev.* **2004**, *24*, 241–266. [CrossRef]
112. Vallance, J.; Boiron, M.-L.; Cathelineau, M.; Fourcade, S.; Varlet, M.; Marignac, C. The granite hosted gold deposit of Moulin de Cheni (Saint-Yrieix district, Massif Central, France): Petrographic, structural, fluid inclusion and oxygen isotope constraints. *Miner. Depos.* **2004**, *39*, 265–281.
113. Miao, L.C.; Qiu, Y.M.; Fan, W.M.; Zhang, F.Q.; Zhai, M.G. Geology, geochronology, and tectonic setting of the Jiapigou gold deposits, southern Jilin Province, China. *Ore Geol. Rev.* **2004**, *26*, 137–165. [CrossRef]
114. Yang, F.Q.; Mao, J.W.; Wang, Y.T.; Bierlein, F.P. Geology and geochemistry of the Bulong quartz–barite vein-type gold deposit in the Xinjiang Uygur Autonomous Region, China. *Ore Geol. Rev.* **2005**, *26*, 52–76.

115. Kreuzer, O.P. Intrusion-hosted mineralization in the Charters Towers goldfield, North Queensland: New isotopic and fluid inclusion constraints on the timing and origin of the auriferous veins. *Econ. Geol.* **2005**, *100*, 1583–1603. [[CrossRef](#)]
116. Xu, J.; Ding, R.; Xie, Y.; Zhong, C.; Shan, L. The source of hydrothermal fluids for the Sarekoubu gold deposit in the southern Altai, Xinjiang, China: Evidence from fluid inclusions and geochemistry. *J. Asian Earth Sci.* **2008**, *32*, 247–258. [[CrossRef](#)]
117. Yang, F.Q.; Mao, J.W.; Bierlein, F.P.; Pirajno, F.; Zhao, C.S.; Ye, H.S.; Liu, F. A review of the geological characteristics and geodynamic mechanisms of Late Paleozoic epithermal gold deposits in North Xinjiang, China. *Ore Geol. Rev.* **2009**, *35*, 217–234. [[CrossRef](#)]
118. Zhang, D.Q.; She, H.Q.; Feng, C.Y.; Li, D.X.; Li, J.W. Geology, age, and fluid inclusions of the Tanjianshan gold deposit, western China: Two orogenies and two gold mineralizing events. *Ore Geol. Rev.* **2009**, *36*, 250–263.
119. Kontak, D.J.; Kyser, K. A fluid inclusion and isotopic study of an intrusion-related gold deposit (IRGD) setting in the 380 Ma South Mountain Batholith, Nova Scotia, Canada: Evidence for multiple fluid. *Miner. Depos.* **2011**, *46*, 337–363. [[CrossRef](#)]
120. Fu, B.; Kendrick, M.A.; Fairmaid, A.M.; Phillips, D.; Wilson, C.J.L.; Mernagh, T.P. New constraints on fluid sources in orogenic gold deposits, Victoria, Australia. *Contrib. Miner. Pet.* **2012**, *163*, 427–447. [[CrossRef](#)]
121. Ryabukha, M.A.; Gibsher, N.A.; Tomilenko, A.A.; Bulbak, T.A.; Khomenko, M.O.; Sazonov, A.M. P-T-X parameters of metamorphogene and hydrothermal fluids, isotopy and age of the Bogunai gold deposit, southern Yenisei Ridge (Russia). *Russ. Geol. Geophys.* **2015**, *56*, 903–918. [[CrossRef](#)]
122. Lai, J.; Ju, P.; Tao, J.; Yang, B.; Wang, X. Characteristics of fluid inclusions and metallogenesis of annage gold deposit in Qinghai Province, China. *Open J. Geol.* **2015**, *5*, 780–794. [[CrossRef](#)]
123. Liang, Y.; Wang, G.; Liu, S.; Sun, Y.; Huang, Y.; Hoshino, K. A Study on the mineralization of the Woxi Au-Sb-W deposit, Western Hunan, China. *Resour. Geol.* **2015**, *65*, 27–38. [[CrossRef](#)]
124. Xu, Y.-F.; Pei, N.P.; Wang, G.-G.; Pan, J.-Y.; Guan, S.-J.; Chen, H.; Ding, J.-Y.; Li, L. Geology, fluid inclusion and stable isotope study of the Huangshan orogenic gold deposit: Implications for future exploration along the Jiangshan-Shaoxing fault zone, South China. *J. Geochem. Explor.* **2016**, *171*, 37–54. [[CrossRef](#)]
125. Chai, P.; Sun, J.-G.; Xing, S.-W.; Li, B.; Lu, C. Ore geology, fluid inclusion and  $^{40}\text{Ar}/^{39}\text{Ar}$  geochronology constraints on the genesis of the Yingchengzi gold deposit, southern Heilongjiang Province, NE China. *Ore Geol. Rev.* **2016**, *72*, 1022–1036. [[CrossRef](#)]
126. Fuertes-Fuente, M.; Cepedal, A.; Lima, A.; Dória, A.; dos Ribeiro, M.A.; Guedes, A. The Au-bearing vein system of the Limarinho deposit (northern Portugal): Genetic constraints from Bi-chalcogenides and Bi-Pb-Ag sulfosalts, fluid inclusions and stable isotopes. *Ore Geol. Rev.* **2016**, *72*, 213–231. [[CrossRef](#)]
127. Khomenko, M.O.; Gibsher, N.A.; Tomilenko, A.A.; Bul'bak, T.A.; Ryabukha, M.A.; Semenova, D.V. Physicochemical parameters and age of the Vasil'kovskoe gold deposit, Northern Kazakhstan. *Russ. Geol. Geophys.* **2016**, *57*, 1728–1749. [[CrossRef](#)]
128. Prokofiev, V.Y.; Safonov, Y.G.; Lüders, V.; Borovikov, A.A.; Kotov, A.A.; Zlobina, T.M.; Murashov, K.Y.; Yudovskaya, M.A.; Selektor, S.L. The sources of mineralizing fluids of orogenic gold deposits of the Baikal-Patom and Muya areas, Siberia: Constraints from the C and N stable isotope compositions of fluid inclusions. *Ore Geol. Rev.* **2019**, *111*, 102988. [[CrossRef](#)]
129. Prokofiev, V.Y.; Afanas'yeva, Z.B.; Ivanova, G.F.; Boiron, M.C.; Marignac, C. Fluid inclusions in mineral at the Olympiada Au-(Sb-W) deposit, Yenisey ridge. *Geochem. Intern.* **1995**, *32*, 104–121.
130. Coutinho, M.G.N.; Alderton, D.H.M. Character and genesis of Proterozoic shear zone-hosted gold deposits in Borborema Province, northeast Brazil. *Transact. Inst. Min. Metall. Sect. B* **1998**, *107*, B109–B119.
131. Genkin, A.D.; Wagner, F.E.; Krylova, T.L.; Tsepina, A.I. Gold-bearing arsenopyrite and its formation condition at the Olympiada and Veduga gold deposits (Yenisei Range, Siberia). *Geol. Ore Depos.* **2002**, *44*, 52–68.
132. Alm, E.; Broman, C.; Billstrom, K.; Sundblad, K.; Torssander, P. Fluid characteristics and genesis of early Neoproterozoic orogenic gold-quartz veins in the Harnas area, southwestern Sweden. *Econ. Geol.* **2003**, *98*, 1311–1328. [[CrossRef](#)]
133. Ferrari, M.A.D.; Choudhuri, A. Structural controls on gold mineralisation and the nature of related of the Paiol gold deposit, Almas Greenstone Belt, Brazil. *Ore Geol. Rev.* **2004**, *24*, 173–197. [[CrossRef](#)]
134. Fraser, G.L.; Skirrow, R.G.; Schmidt-Mumm, A.; Holm, O. Mesoproterozoic gold in the central Gawler craton, South Australia: Geology, alteration, fluids, and timing. *Econ. Geol.* **2007**, *102*, 1511–1539. [[CrossRef](#)]

135. Budd, A.R.; Skirrow, R.G. The nature and origin of gold deposits of the Tarcoola Goldfield and implications for the central Gawler gold province, South Australia. *Econ. Geol.* **2007**, *102*, 1541–1563. [[CrossRef](#)]
136. Schindler, C.; Hagemann, S.G.; Banks, D.; Mernagh, T.; Harris, A.C. Magmatic hydrothermal fluids at the sedimentary rock-hosted, intrusion-related telfer gold–copper deposit, paterson orogen, Western Australia: Pressure–temperature–composition constraints on the ore-forming fluids. *Econ. Geol.* **2016**, *111*, 1099–1126. [[CrossRef](#)]
137. Fedorowich, J.; Stauffer, M.; Kerrich, R. Structural setting and fluid characteristics of the Proterozoic tartan lake gold deposit, trans-hudson orogen, northern Manitoba. *Econ. Geol.* **1991**, *86*, 1434–1467. [[CrossRef](#)]
138. Ibrahim, M.S.; Kyser, T.K. Fluid inclusion and isotope systematics of the high-temperature Proterozoic Star Lake lode gold deposit, Northern Saskatchewan, Canada. *Econ. Geol.* **1991**, *86*, 1468–1490. [[CrossRef](#)]
139. Ansdell, K.M.; Kyser, T.K. Mesothermal gold mineralization in a Proterozoic greenstone belt: Western Flin Flon Domain, Saskatchewan, Canada. *Econ. Geol.* **1992**, *87*, 1496–1524. [[CrossRef](#)]
140. Poutainen, M. Fluid inclusion geochemistry of the early Proterozoic Piril i gold deposit in Rantasalmi, southeastern Finland. *Miner. Depos.* **1993**, *28*, 129–135. [[CrossRef](#)]
141. Field, M.P.; Kerrich, R.; Kyser, T.K. Characteristics of barren quartz veins in the Proterozoic La Ronge Domain, Saskatchewan, Canada: A comparison with auriferous counterparts. *Econ. Geol.* **1998**, *93*, 602–616. [[CrossRef](#)]
142. Klein, E.L.; Fuzikawa, K.; Koppe, J.C.; Dantas, M.S.S. Fluid associated with the Caxias mesothermal gold mineralization, São Luis craton, northern Brazil: A fluid inclusion study. *Rev. Bras. Geocienc.* **2000**, *30*, 322–326. [[CrossRef](#)]
143. Xavier, R.P.; Coelho, C.E.S. Fluid regimes related to the formation of lode–gold deposits in Rio Itapicuru Greenstone Belt, Bahia: A fluid inclusion review. *Rev. Bras. Geocienc.* **2000**, *30*, 311–314. [[CrossRef](#)]
144. Klein, E.L.; dos Santos, R.A.; Fuzikawa, K.; Angelica, R.S. Hydrothermal fluid evolution and structural control of the Guarim gold mineralisation, Tapajos Province, Amazonian Craton, Brazil. *Miner. Depos.* **2001**, *36*, 149–164. [[CrossRef](#)]
145. Hein, K.A.A.; Zaw, K.; Mernagh, T.P. Linking mineral and fluid inclusion paragenetic studies: The Batman deposit, Mt. Todd (Yimuyn Manjerr) goldfield, Australia. *Ore Geol. Rev.* **2006**, *28*, 180–200. [[CrossRef](#)]
146. Klein, E.L.; Harris, C.; Renac, C.; Giret, A.; Moura, C.A.; Fuzikawa, K. Fluid inclusion and stable isotope (O, H, C, and S) constraints on the genesis of the Serrinha gold deposit, Gurupi belt, northern Brazil. *Miner. Depos.* **2006**, *41*, 160–178. [[CrossRef](#)]
147. Mernagh, T.P.; Wygralak, A.S. Gold ore-forming of the Tanami region, Northern Australia. *Miner. Depos.* **2007**, *42*, 145–173. [[CrossRef](#)]
148. Coullbaly, Y.; Boiron, M.C.; Cathelineau, M.; Kouamelan, A.N. Fluid immiscibility and gold deposition in the Birimian quartz veins of the Angovia deposit (Yaoure, Ivory Coast). *J. Afr. Earth Sci.* **2008**, *50*, 234–254. [[CrossRef](#)]
149. Klein, E.L.; Ribeiro, J.W.A.; Harris, C.; Moura, C.A.V.; Giret, A. Geology and fluid characteristics of the Mina Velha and Mandiocal orebodies and implications for the genesis of the orogenic Chega Tudo gold deposit, Gurupi Belt, Brazil. *Econ. Geol.* **2008**, *103*, 957–980. [[CrossRef](#)]
150. Billstrom, K.; Broman, C.; Jonsson, E.; Recio, C.; Boyce, A.J.; Torssander, P. Geochronological, stable isotopes and fluid inclusion constraints for a premetamorphic development of the intrusive-hosted Bjorkdal Au deposit, northern Sweden. *Intern. J. Earth Sci.* **2009**, *98*, 1027–1052. [[CrossRef](#)]
151. Klein, E.L.; Fuzikawa, K. Origin of the CO<sub>2</sub>-only fluid inclusions in the Palaeoproterozoic Carara vein-quartz gold deposit, Ipitinga Auriferous District, SE-Guiana Shield, Brazil: Implications for orogenic gold mineralization. *Ore Geol. Rev.* **2010**, *37*, 31–40. [[CrossRef](#)]
152. Hammond, N.Q.; Robb, L.; Foya, S.; Ishiyama, D. Mineralogical, fluid inclusion and stable isotope characteristics of Birimian orogenic gold mineralization at the Morila mine, Mali, West Africa. *Ore Geol. Rev.* **2011**, *39*, 218–229. [[CrossRef](#)]
153. Lawrence, D.M.; Treloar, P.J.; Rankin, A.H.; Boyce, A.; Harbridge, P. A fluid inclusion and stable isotope study at the Loulo mining district, Mali, West Africa: Implications for multifluid sources in the generation of orogenic gold deposits. *Econ. Geol.* **2013**, *108*, 229–257. [[CrossRef](#)]
154. de Freitas, S.C.F.; Klein, E.L. The mineralizing fluid in the Piaba gold deposit, São Luís cratonic fragment (NW-Maranhão, Brazil) based on fluid inclusion studies in quartz veins. *Braz. J. Geol.* **2013**, *43*, 70–84. [[CrossRef](#)]

155. Tassinari, C.C.G.; Mateus, A.M.; Velásquez, M.E.; Munhá, J.M.U.; Lobato, L.M.; Bello, R.M.; Chiquini, A.P.; Campos, W.F. Geochronology and thermochronology of gold mineralization in the Turmalina deposit, NE of the Quadrilátero Ferrífero Region, Brazil. *Ore Geol. Rev.* **2015**, *67*, 368–381. [[CrossRef](#)]
156. Klein, E.L.; Lucas, F.R.A.; Queiroz, J.D.S.; Freitas, S.C.F.; Renac, C.; Galarza, M.A.; Jourdan, F.; Armstrong, R. Metallogenesis of the Paleoproterozoic Piaba orogenic gold deposit, São Luís cratonic fragment, Brazil. *Ore Geol. Rev.* **2015**, *65*, 1–25. [[CrossRef](#)]
157. Ampsonah, P.O.; Salvi, S.; Beziat, D.; Siebenaller, L.; Baratoux, L.; Jessell, M.W. Geology and geochemistry of the shear-hosted Julie gold deposit, NW Ghana. *J. Afr. Earth Sci.* **2015**, *112*, 505–523. [[CrossRef](#)]
158. Morales, M.J.; Figueiredo e Silva, R.C.; Lobato, L.M.; Gomes, S.D.; Gomes, C.C.C.O.; Banks, D.A. Metal source and fluid–rock interaction in the Archean BIF-hosted Lamego gold mineralization: Microthermometric and LA-ICP-MS analyses of fluid inclusions in quartz veins, Rio das Velhas greenstone belt, Brazil. *Ore Geol. Rev.* **2016**, *72*, 510–531. [[CrossRef](#)]
159. Guha, J.; Leroy, J.; Guha, D. Significance of fluid phases associated with shear zone Cu–Au mineralisation in the Dore lake complex, Chibougamau, Quebec. *Bull. Mineral.* **1979**, *102*, 569–576. [[CrossRef](#)]
160. Smith, T.J.; Cloke, P.L.; Kesler, S.E. Geochemistry of fluid inclusions from the McIntyre-Hollinger gold deposit, Timmins, Ontario, Canada. *Econ. Geol.* **1984**, *79*, 1265–1285. [[CrossRef](#)]
161. Santosh, M. Ore fluids in the auriferous champion reef of kolar, South India. *Econ. Geol.* **1986**, *81*, 1546–1552. [[CrossRef](#)]
162. Studemeister, P.A.; Kilias, S. Alteration pattern and fluid inclusions of gold-bearing quartz veins in Archean trondjemite near Wawa, Ontario, Canada. *Econ. Geol.* **1987**, *82*, 429–439. [[CrossRef](#)]
163. Burrows, D.R.; Spooner, E.T.C. Generation of a magmatic H<sub>2</sub>O–CO<sub>2</sub> fluid enriched in Mo, Au, and W within an Archean sodic granodiorite stock, Mink Lake, northwestern Ontario. *Econ. Geol.* **1987**, *82*, 1931–1957. [[CrossRef](#)]
164. Robert, F.; Kelly, W.C. Ore-forming fluids in archean gold-bearing quartz veins at the sigma mine, abitibi greenstone belt, Quebec, Canada. *Econ. Geol.* **1987**, *82*, 1464–1482. [[CrossRef](#)]
165. Naumov, V.B.; Safonov, Y.G.; Mironova, O.F. Some regularities in spatial variations of the parameters of fluid of the Kolar gold deposit, India. *Geol. Rudn. Mestorozhd* **1988**, *6*, 105–109.
166. Walsh, J.F.; Kesler, S.E.; Duff, D.; Cloke, P.L. Fluid inclusion geochemistry of high-grade, vein-hosted gold ore at the Pamour mine, Porcupine camp, Ontario. *Econ. Geol.* **1988**, *83*, 1347–1367. [[CrossRef](#)]
167. De Ronde, C.E.J.; Spooner, E.T.C.; De Wit, M.J.; Bray, C.J. Shear zone-related, Au quartz vein deposits in the Barberton greenstone belt, South Africa: Field and petrographic characteristics, fluid properties and light stable isotope geochemistry. *Econ. Geol.* **1992**, *87*, 366–402. [[CrossRef](#)]
168. Samson, I.M.; Bas, B.; Holm, P.E. Hydrothermal evolution of auriferous shear zones, Wawa, Ontario. *Econ. Geol.* **1997**, *92*, 325–342. [[CrossRef](#)]
169. Boullier, A.-M.; Firdaous, K.; Robert, F. On the significance of aqueous fluid inclusions in gold-bearing quartz vein deposits from the southeastern Abitibi subprovince (Quebec, Canada). *Econ. Geol.* **1998**, *93*, 216–233. [[CrossRef](#)]
170. Mishra, B.; Panigrahi, M.K. Fluid evolution in the Kolar Gold Field: Evidence from fluid inclusion studies. *Miner. Depos.* **1999**, *34*, 173–181. [[CrossRef](#)]
171. Hagemann, S.G.; Luders, V. Antimony–gold mineralization at the epizonal Wiluna lode-gold deposits, Western Australia: Infrared microthermometric constraints on the P–T–X conditions of stibnite mineralization. In *Terra Nostra ECROFI XV Abstract and Program*; GeoForschungsZentrum (GFZ): Potsdam, Germany, 1999; pp. 140–142.
172. Dugdale, A.L.; Hagemann, S.G. The Bronzewing lode–gold deposit, Western Australia: P–T–X evidence for fluid immiscibility caused by cyclic decompression in gold-bearing quartz-veins. *Chem. Geol.* **2001**, *173*, 59–90. [[CrossRef](#)]
173. Olivo, G.R.; Williams-Jones, A.E. Genesis of the auriferous C quartz-tourmaline vein of the Siscoe mine, Val d’Or district, Abitibi subprovince, Canada: Structural, mineralogical and fluid inclusion constraints. *Econ. Geol.* **2002**, *97*, 929–947. [[CrossRef](#)]
174. Polito, P.A.; Bone, Y.; Clarke, J.D.A.; Mernagh, T.P. Compositional zoning of fluid inclusions in the Archean Junction gold deposit, Western Australia: A process of fluid-wall-rock interaction? *Aust. J. Earth Sci.* **2001**, *48*, 833–855. [[CrossRef](#)]

175. Blewett, R.S.; Huston, D.L.; Mernagh, T.P.; Kamprad, J. The diverse structure of Archean lode gold deposits of the southwest Mosquito Creek belt, East Pilbara Craton, Western Australia. *Econ. Geol.* **2002**, *97*, 787–800. [[CrossRef](#)]
176. Neumayr, P.; Hagemann, S.G. Hydrothermal fluid evolution within the Cadillac tectonic zone, Abitibi greenstone belt, Canada: Relationship to auriferous fluids in adjacent second- and third-order shear zones. *Econ. Geol.* **2002**, *97*, 1203–1225. [[CrossRef](#)]
177. Pal, N.; Mishra, B. Alteration geochemistry and fluid inclusion characteristics of the greenstone-hosted gold deposit of Huttī, Eastern Dharwar Craton, India. *Miner. Depos.* **2002**, *37*, 722–736. [[CrossRef](#)]
178. Uemoto, T.; Ridley, J.; Mikucki, E.; Groves, D.I.; Kusakabe, M. Fluid chemical evolution as a factor in controlling the distribution of gold at the Archean Golden Crown lode gold deposit, Murchison province, Western Australia. *Econ. Geol.* **2002**, *97*, 1227–1248. [[CrossRef](#)]
179. Hagemann, S.G.; Luders, V. P-T-X conditions of hydrothermal fluids and precipitation mechanism of stibnite-gold mineralization at the Wiluna lode-gold deposits, Western Australia: Conventional and infrared microthermometric constraints. *Miner. Depos.* **2003**, *8*, 936–952. [[CrossRef](#)]
180. Poutiainen, M.; Partamies, S. Fluid evolution of the late Archean Ramepuro gold deposit in the Ilomantsi greenstone belt in eastern Finland. *Miner. Depos.* **2003**, *38*, 196–207. [[CrossRef](#)]
181. Zhou, T.; Phillips, G.N.; Denn, S.; Burke, S. Woodcutters goldfield: Gold in an archaean granite, Kalgoorlie, Western Australia. *Aust. J. Earth Sci.* **2003**, *50*, 553–569. [[CrossRef](#)]
182. Baker, D.E.L.; Seccombe, P.K. Physical conditions of gold deposition at the McPhees deposit, Pilbara Craton, western Australia: Fluid inclusion and stable isotope constraints. *Can. Miner.* **2004**, *42*, 1405–1441. [[CrossRef](#)]
183. Duuring, P.; Hagemann, S.G.; Cassidy, K.F.; Johnson, C.A. Hydrothermal alteration, ore fluid characteristics, and gold depositional processes along a trondhjemite–komatiite contact at Tarmoola, Western Australia. *Econ. Geol.* **2004**, *99*, 423–451. [[CrossRef](#)]
184. Mernagh, T.P.; Heinrich, C.A.; Mikucki, E.J. Temperature gradients recorded by fluid inclusions and hydrothermal alteration at the Mount Charlotte gold deposit, Kalgoorlie, Australia. *Can. Miner.* **2004**, *42*, 1383–1403. [[CrossRef](#)]
185. Shelton, K.L.; McMenamy, T.A.; van Hees, E.H.P.; Falck, H. Deciphering the complex fluid history of greenstone-hosted gold deposit: Fluid inclusion and stable isotope studies of the Giant mine, Yellowknife, Northwest Territories, Canada. *Econ. Geol.* **2004**, *99*, 1643–1663. [[CrossRef](#)]
186. Mishra, B.; Pal, N.; Sarbadhikari, A.B. Fluid inclusion characteristics of the Uti gold deposit, Huttī-Maskī greenstone belt, southern India. *Ore Geol. Rev.* **2005**, *26*, 1–16. [[CrossRef](#)]
187. Buchholz, P.; Oberthur, T.; Luders, V.; Wilkinson, J. Multistage Au–As–Sb mineralization and crustal-scale fluid evolution in the Kwekwe district, Midlands greenstone belt, Zimbabwe: A combined geochemical, mineralogical, stable isotope, and fluid inclusion study. *Econ. Geol.* **2007**, *102*, 347–378. [[CrossRef](#)]
188. Mishra, B.; Pal, N. Metamorphism, fluid flux, and fluid evolution relative to gold mineralization in the Huttī-Maskī greenstone belt, eastern Dharwar craton, India. *Econ. Geol.* **2008**, *103*, 801–827. [[CrossRef](#)]
189. Baker, T.; Bertelli, M.; Blenkinsop, T.; Cleverley, J.S.; McLellan, J.; Nugus, M.; Gillen, D. P-T-X conditions of fluids in the Sunrise Dam gold deposit, Western Australia, and implications for the interplay between deformation and fluids. *Econ. Geol.* **2010**, *105*, 873–894. [[CrossRef](#)]
190. Mernagh, T.P.; Bastrakov, E.N. An evaluation of hydrogen sulfide in orogenic gold fluids and the uncertainties associated with vapor-rich inclusions. *Geofluids* **2013**, *13*, 494–505. [[CrossRef](#)]
191. Chinnasamy, S.S.; Uken, R.; Reinhardt, J.; Selby, D.; Johnson, S. Pressure, temperature, and timing of mineralization of the sedimentary rock-hosted orogenic gold deposit at Klipwal, southeastern Kaapvaal Craton, South Africa. *Miner. Depos.* **2015**, *50*, 739–766. [[CrossRef](#)]
192. Ridley, J.R.; Diamond, L.W. Fluid chemistry of orogenic lode gold deposits and implications for genetic models. *Gold 2000 SEG Rev.* **2000**, *13*, 141–162.
193. Bodnar, R.J.; Lecumberri-Sánchez, P.; Moncada, D.; Steele-MacInnes, P. Fluid inclusions in hydrothermal ore deposits. Reference module in earth systems and environmental sciences. In *Treatise on Geochemistry*, 2nd ed.; Elsevier: Amsterdam, The Netherlands, 2014; pp. 119–142.
194. Groves, D.I.; Santosh, M.; Deng, J.; Wang, Q.; Yang, L.; Zhang, L. A holistic model for the origin of orogenic gold deposits and its implications for exploration. *Miner. Depos.* **2019**, 1–18. [[CrossRef](#)]

195. Kesler, S.E.; Wilkinson, B.H. The role of exhumation in the temporal distribution of ore deposits. *Econ. Geol.* **2006**, *101*, 919–922. [[CrossRef](#)]
196. Yardley, B.W.D.; Graham, J.T. The origins of salinity in metamorphic fluids. *Geofluids* **2002**, *2*, 249–256. [[CrossRef](#)]



© 2020 by the authors. Licensee MDPI, Basel, Switzerland. This article is an open access article distributed under the terms and conditions of the Creative Commons Attribution (CC BY) license (<http://creativecommons.org/licenses/by/4.0/>).